(12)

AAE

AERONAUTICAL AND ASTRONAUTICAL ENGINEERING DEPARTMENT

SCALE EFFECTS IN A CW HF

CHEMICAL LASER

L. H. Sentman, D. L. Carroll, P. Theodoropoulos and A. Gumus

ENGINEERING EXPERIMENT STATION, COLLEGE OF ENGINEERING, UNIVERSITY OF ILLINOIS, URBANA

Aeronautical and Astronautical Engineering Department

University of Illinois at Urbana-Champaign

Urbana, Illinois

Technical Report AAE TR 86-5

UILU Eng 86-0505

SCALE EFFECTS IN A CW HF CHEMICAL LASER

L. H. Sentman, D. L. Carroll, P. Theodoropoulos and A. Gumus

Prepared for

Defense Advanced Research Projects Agency

1400 Wilson Blvd.

Arlington, VA 22209

September, 1986

SECURITY CLASSIFICATION OF THIS PAGE (When Data Entered)

REPORT DOCUMENTATION PAGE

READ INSTRUCTIONS BEFORE COMPLETING FORM

1 REPORT NUMBER: AAE 86-5 UILU ENG 86-0505	2 GOVT ACCESSION NO.: AD-A172503
3 RECIPIENT'S CATALOG NUMBER:	
4 TITLE (and Subtitle): Scale Effects in a cw HF Chemical Laser	5 TYPE OF REPORT & PERIOD COVERED: Technical Report
	6 PERFORMING ORG. REPORT NUMBER:
7 AUTHOR(s): L. H. Sentman, D. L. Carroll, P. Theodoropoulos and A. Gamus	8 CONTRACT OR GRANT NUMBER(s): N00014-85-K-0326
9 PERFORMING ORGANIZATION NAME AND ADDRESS: Aeronautical and Astronautical Engineering, University of Illinois at Urbana-Champaign, Urbana, IL 61801	10 PROGRAM ELEMENT, PROJECT, TASK AREA & WORK UNIT NUMBERS:
11 CONTROLLING OFFICE NAME AND ADDRESS: Defense Advanced Research Projects Agency, 1400 Wilson Boulevard, Arlington, VA 22209	12 REPORT DATE: September 19
	13 NUMBER OF PAGES:
14 MONITORING AGENCY NAME & ADDRESS (if different from Controlling Office): Office of Naval Research, Resident Representative, Room 286, 536 South Clark Street, Chicago, IL 60605	15 SECURITY CLASS (of this report): UNCLASSIFIED
	15a DECLASSIFICATION DOWNGRADING SCHEDULE:

16 DISTRIBUTION STATEMENT (of this Report)

UNLIMITED

DISTRIBUTION STATEMENT A
Approved for public release
Distribution Unlimited

17 DISTRIBUTION STATEMENT (of the abstract entered in Block 20, if different from Report)

18 SUPPLEMENTARY NOTES

19 KEY WORDS (Continue on reverse side if necessary and identify by block number)

Chemical laser
Scale effects with constant saturated gain
Scale effects with constant cavity loss
Time-dependent oscillations
Unstable resonator

20 ABSTRACT (Continue on reverse side if necessary and identify by block number)

Scale effects when the size of a cw HF chemical laser was reduced by a factor of two were studied experimentally and theoretically. When the saturated gains of the single channel CL I laser and the two channel CL II laser were the same, the CL I power was 70-80% of the CL II power. This suggests that for only a 25% performance penalty, the size, weight and gas requirements of a laser can be reduced by a factor of two. The power spectral distributions of the CL I and CL II lasers when the saturated gains were the

DD FORM 1 JAN 73 1473 EDITION OF 1 NOV 65 IS OBSOLETE

SECURITY CLASSIFICATION OF THIS PAGE (When Data Entered)

20. ABSTRACT

same were nearly identical. When the two lasers had the same cavity losses, the CL I power was an average of 45% of the CL II power. The Blaze II and MNORO3SR laser computer simulations gave good agreement with data as a function of mass flow rate, cavity losses, pressure and size of the laser. Time-dependent oscillations on lines whose saturated gain did not fill the unstable resonator had a period of 47 ns. These oscillations did not occur for Fresnel numbers less than 3.2 and their amplitudes increased as the fraction of the resonator filled by the saturated gain of the oscillating line decreased. A 7 ns oscillation, which was superimposed on top of the 47 ns oscillation, was probably a mode beat of the laser.

TABLE OF CONTENTS

I. INTRODUCTION

This research is an integrated experimental and theoretical investigation of the multi-line issues associated with assessing the impact of temporal variations in a cw HF device on the capability of achieving a phased output beam from multiple laser cavities. The objectives of this research are to fully characterize the output of an oscillator-amplifier (MOPA) configuration as a function of the oscillator input beam, time-dependent oscillations, mode beats, and determine if the coupling between the oscillator and amplifier perturbs the oscillator output; these studies are to be carried out for first one and then two amplifiers driven by the same oscillator. To accomplish these objectives, the flow fields in the oscillator and amplifiers must be identical. To ensure that this is so, the devices must first be fully characterized as oscillators (power, power spectral distributions, beam diameters, time-dependent oscillations as a function of cavity losses, pressure and flow rates) including simulation of their performance with computer models. This background information is essential to the interpretation and guidance of the MOPA experiments.

The two channel Helios CL II cw HF chemical laser, which will be used as the amplifier, was fully characterized in a previous study of the time-dependent oscillations which occur on lines whose saturated gain does not fill the unstable resonator[1-8]. The flow channel in the single channel Helios CL I cw HF laser, which will be used as the oscillator, is identical to one of the flow channels in the two channel laser which will be used as the amplifier. Thus, when the CL I is run at one half the mass flow rates of the CL II, the flow fields in the oscillator and amplifier are identical. The objective of this study was to fully characterize the Helios CL I single channel laser as

an oscillator. To facilitate comparison with the CL II data, power, power spectral distributions, beam diameters, and time-dependent oscillations as a function of cavity losses, pressure and flow rates were measured for the same range of parameters for which the CL II data were taken.

Comparison of the two lasers when the cavity losses were the same showed that the CL I stable resonator power was an average of 45% of the CL II stable resonator power. The power split between vibrational bands remained about the same while the peaks of the CL I power spectral distributions were shifted one J lower than the CL II spectral peaks. The CL I spectra exhibit fewer J lines than CL II spectra. The CL I beam diameters were smaller than the CL II beam diameters. All of these scale effects are a consequence of the fact that the saturated gain of the CL I laser was twice that of the CL II laser when the two lasers have the same cavity loss.

Comparison of CL I and CL II stable resonator performance when the saturated gains were the same showed that the CL I power was 52-80% of the CL II power; for the high SF_6 flow rates, the CL I power was 70-80% of the CL II power. These data indicate that, if the saturated gain is kept constant as the size of the laser is reduced, it may be possible to reduce the size, weight and gas requirements by a factor of two with only a 25% performance penalty. The power spectral distributions of the two lasers were similar when the saturated gains were the same.

To verify the ability of the Blaze II[9] and MNORO3SR[7] computer simulations of the Helios laser to predict performance as the size of the laser changes, CL I simulations were made by halving the input mass flow rates and gain length of the CL II laser. The results of these calculations gave good agreement with the measured CL I power, power split and beam diameters. MNORO3SR computations produced power spectral distributions which are a

reasonable agreement with the CL I data. These calculations show that the Blaze II and MNORO3SR simulations of the Helios laser are valid as a function of mass flow rate, cavity losses, pressure and size of the laser.

To complete the characterization of the CL I laser, the CL I was run with an unstable resonator. These experiments used a 50% geometric outcoupled, confocal, unstable resonator. A variable slit scraper mirror was used to outcouple the power and allowed the Fresnel number to vary from 0.0 to 35.7. The time-dependent oscillations in the output beam of the CL I unstable resonator all had a period of about 47 ns and increased in amplitude as the fraction of the resonator filled by the saturated gain of a lasing line decreased. A 7 ns oscillation, which was superimposed on top of the 47 ns oscillation, is thought to be a mode beat of the laser. The oscillations on lines whose saturated gain does not fill the resonator did not occur for Fresnel numbers less than 3.2. Overall, the CL I unstable resonator data is consistent with the CL II unstable resonator data.

Section II presents the CL I stable resonator data, compares it to computer simulations and to CL II data and CL II simulations. Section III presents the CL I unstable resonator data and compares it with the CL II unstable resonator data. In Section IV, several concluding remarks are presented.

II. CL I STABLE RESONATOR PERFORMANCE

To study the performance of a Master Oscillator Power Amplifier (MOPA) configuration as a function of the characteristics of the oscillator and the amplifier, the behavior of each of these devices must first be understood when they are operated as oscillators. The two channel Helios CL II laser, which will be used as the amplifier, has been completely characterized as an oscillator in previous studies[1-8]. The oscillator to be used in the MOPA experiments will be a single channel Helios CL I laser. The flow channel of the CL I laser is identical to one of the flow channels of the CL II laser. This permits the flow fields of the oscillator and amplifier to be identical when the CL I laser is run at one half the flow rates of the CL II amplifier. The characterization of the CL I as an oscillator is presented in this report.

The CL I laser was characterized with a stable resonator for three different cavity losses, for low and high cavity pressures, and for six combinations of SF_6 and H_2 flow rates. Scale effects were determined by comparing CL I laser data with CL II laser data. These comparisons were made for the two lasers having the same cavity losses and for the two lasers having the same saturated gain. The latter comparison is of particular interest because it indicates that a 50% reduction in the laser size, weight and gas requirements results in only a 25 performance penalty.

2.1 EXPERIMENTAL STABLE RESONATOR PERFORMANCE

The CL I laser is a single flow channel, arc driven, cw, subsonic HF chemical laser. The geometry of the flow channel is identical to the geometry of one of the flow channels of the two channel CL II laser (see Reference 5 for a complete description of the CL II laser). To fully characterize the CL I, power, power spectral distributions, beam diameters, and cavity pressures

were measured for six combinations of SF_6 and H_2 flow rates, for high and low cavity pressures, and for three different cavity losses. The mass flow rates used for the CL I were exactly half of the mass flow rates used for the CL II. For corresponding flow rates, the cavity pressures in the CL I were adjusted to be the same as in the CL II. The stable resonator used consisted of two concave 2 meter radius of curvature mirrors. The feedback mirror was always an enhanced total reflector (ETR, r = 0.995 +). The outcoupler was a zinc selenide, partial reflector of either 46% or 63% reflectivity.

2.1.1 EXPERIMENTAL PROCEDURE

The total multiline power was measured by placing a Scientech Model 362 power meter into the outcoupled beam after the total power of the beam was reduced by 90% by a chopper, Figure 1.

The pressure in the laser cavity was adjusted by a flow control valve. The flow control valve was partially closed to achieve cavity pressures in the 5-7 torr range; the flow control valve was closed further to obtain cavity pressures in the 10-12 torr range. The pressure in the cavity was measured by a digital readout connected to a Baratron pressure gauge which in turn was connected to a centerline pressure tap in the laser cavity, 5 mm downstream of the H_2 injectors.

In previous[1-5] studies, a strip chart recorder had been used to take spectra. For the present studies, the spectra were taken with a Tektronix MP2501 data acquisition system, Figure 1. This data acquisition equipment consists of two 7854 digitizing oscilloscopes, a 4041 computer, 4105 display terminal, two P6202A FET probes, and a 4695 graphics printer. To acquire, store and plot the power spectral distributions, several subroutines were written and added to the original MP2501 software.

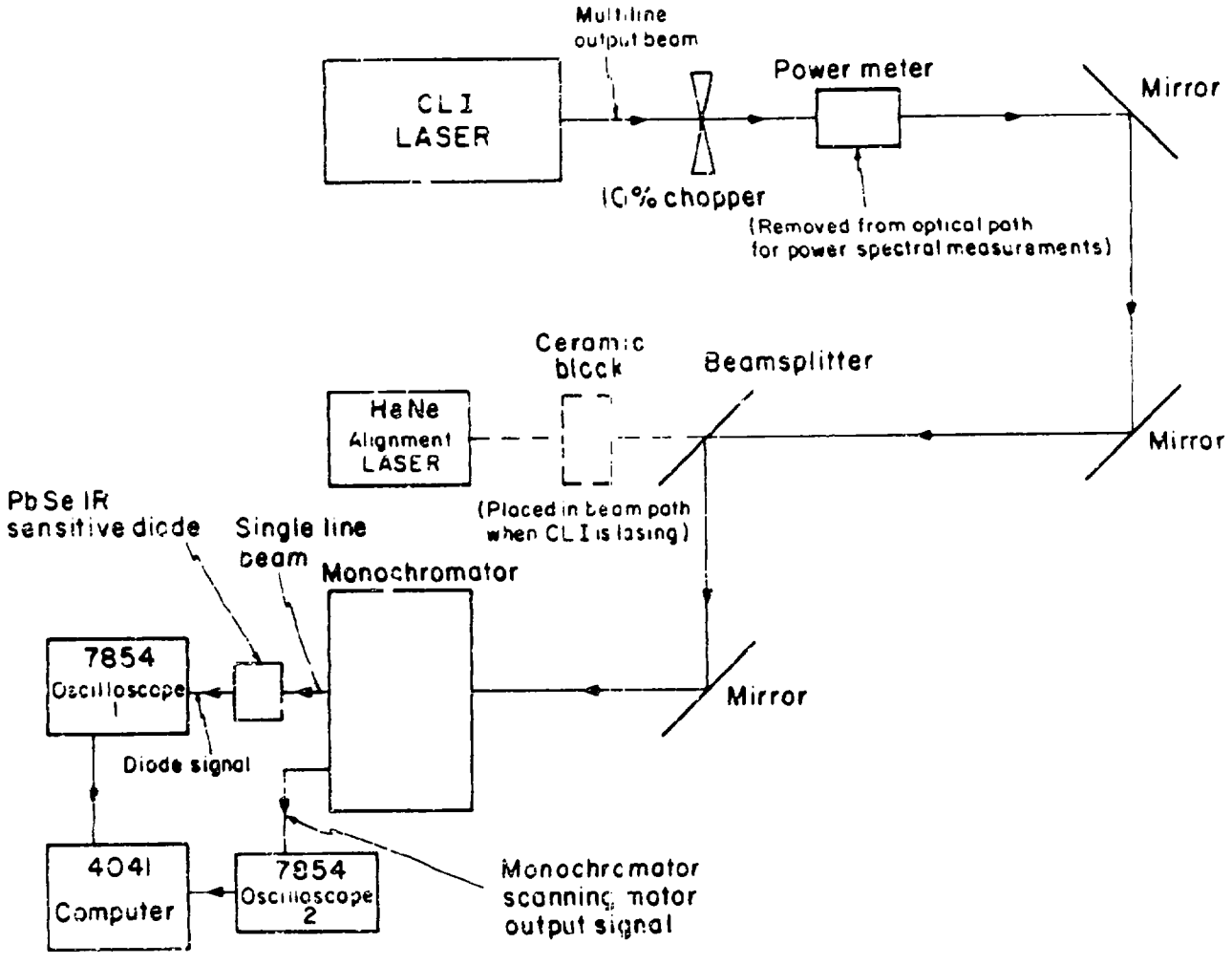

Figure 1. Schematic of the experiment layout for power and power spectral measurements for the Helios CL I laser.

For all runs, two burn blocks were taken, one near the outcoupler and one far from it. The beam diameter at the outcoupling mirror was extrapolated for all runs using the divergence angle determined from these two burn blocks.

2.1.2 STABLE RESONATOR IN VACUUM MIRROR MOUNTS (VMM), r_{eff} = 0.46

The stable resonator used the 46% partially reflective outcoupler and the ETR in vacuum mirror mounts (VMM) attached to the laser body. The distance between the mirrors was 32.7 cm. Using a HeNe laser, the resonator is initially aligned with the optical axis 1.3 mm downstream of the H_2 injectors. When the laser is in operation, the mirrors are tuned for maximum power and thus, the exact location of the optical axis at maximum power is unknown.

The peak power, fraction of the power in the 1→0 vibrational band and the beam diameter for the six combinations of SF_6 and H_2 flow rates for the low and high pressure cases are summarized in Tables 1 and 2, respectively. The power spectral distributions for these six flow rates for low and high pressures are shown in Figures 2 through 5. The power spectral distributions show that the spectra shift toward higher J lines as the SF_6 flow rate is increased. This shift is caused by the increase in temperature of the lasant medium, which accompanies the increased heat release due to the increased F atom flow rate[4]. Comparison of high and low pressure power spectral distributions shows that, for a fixed flow rate there is a shift in the spectra toward higher J lines as pressure increased. This shift in the spectra is a consequence of rotational relaxation. The rotational relaxation rate is proportional to pressure squared, so as pressure increases, the rotational relaxation rate increases, thus producing a more rotationally relaxed spectra which is seen as a shift toward higher J lines.

r_{eff} = 0.46, Low P

RUN NO.	32	33	34	35	36	37
$\dot{m}_{H_2}$ (gm/sec)	0.0228	0.0228	0.0228	0.0305	0.0305	0.0305
$\dot{m}_{SF_6}$ (gm/sec)	0.715	0.535	0.355	0.715	0.535	0.355
Blaze II (Input Data)						
% SF_6 Dissoc.	3.3	4.0	4.0	3.3	4.0	4.0
Initial T (°K)	500	450	450	500	450	450
H_2 Mixing Length	3.0	3.5	4.0	3.0	3.5	4.0
P (Meas.) (Torr)	6.7	6.0	5.4	7.2	6.5	5.8
P_T (Watts)						
Data	25.4	16.7	11.7	28.0	18.2	12.6
Blaze II	22.1	21.4	14.4	23.7	22.8	15.3
P_{10}/P_T						
Data	0.496	0.409	0.352	0.460	0.470	0.412
Blaze II	0.502	0.487	0.475	0.499	0.488	0.475
Beam Dia. (mm)						
Data	2.55	2.81	3.67	2.83	2.76	3.34
Blaze II	4.61	5.03	5.21	3.63	4.03	4.20

Table 1. Summary of the low pressure stable resonator data and Blaze II results for the Helios CL I with a 46% reflective outcoupler in VMM.

r_{eff} = 0.46, High P

RUN NO.	32	33	34	35	36	37
$\dot{m}_{H_2}$ (gm/sec)	0.0228	0.0228	0.0228	0.0305	0.0305	0.0305
$\dot{m}_{SF_6}$ (gm/sec)	0.715	0.535	0.355	0.715	0.535	0.355
Blaze II (Input Data)						
% SF_6 Dissoc.	3.3	4.0	4.0	3.3	4.0	4.0
Initial T (°K)	500	450	450	500	450	450
H_2 Mixing Length	3.0	3.5	4.0	3.0	3.5	4.0
P (Meas.) (Torr)	11.5	10.7	10.0	12.3	11.6	10.7
P_T (Watts)						
Data	17.8	15.0	9.0	20.0	16.7	10.3
Blaze II	16.8	16.9	13.2	19.1	18.9	14.3
P_{10}/P_T						
Data	0.613	0.486	0.463	0.654	0.583	0.441
Blaze II	0.536	0.511	0.496	0.528	0.509	0.495
Beam Dia. (mm)						
Data	2.08	2.36	1.62	2.22	2.47	3.02
Blaze II	3.06	3.26	3.12	2.48	2.63	2.59

Table 2. Summary of the high pressure stable resonator data and Blaze II results for the Helios CL I with a 46% reflective outcoupler in VMM.

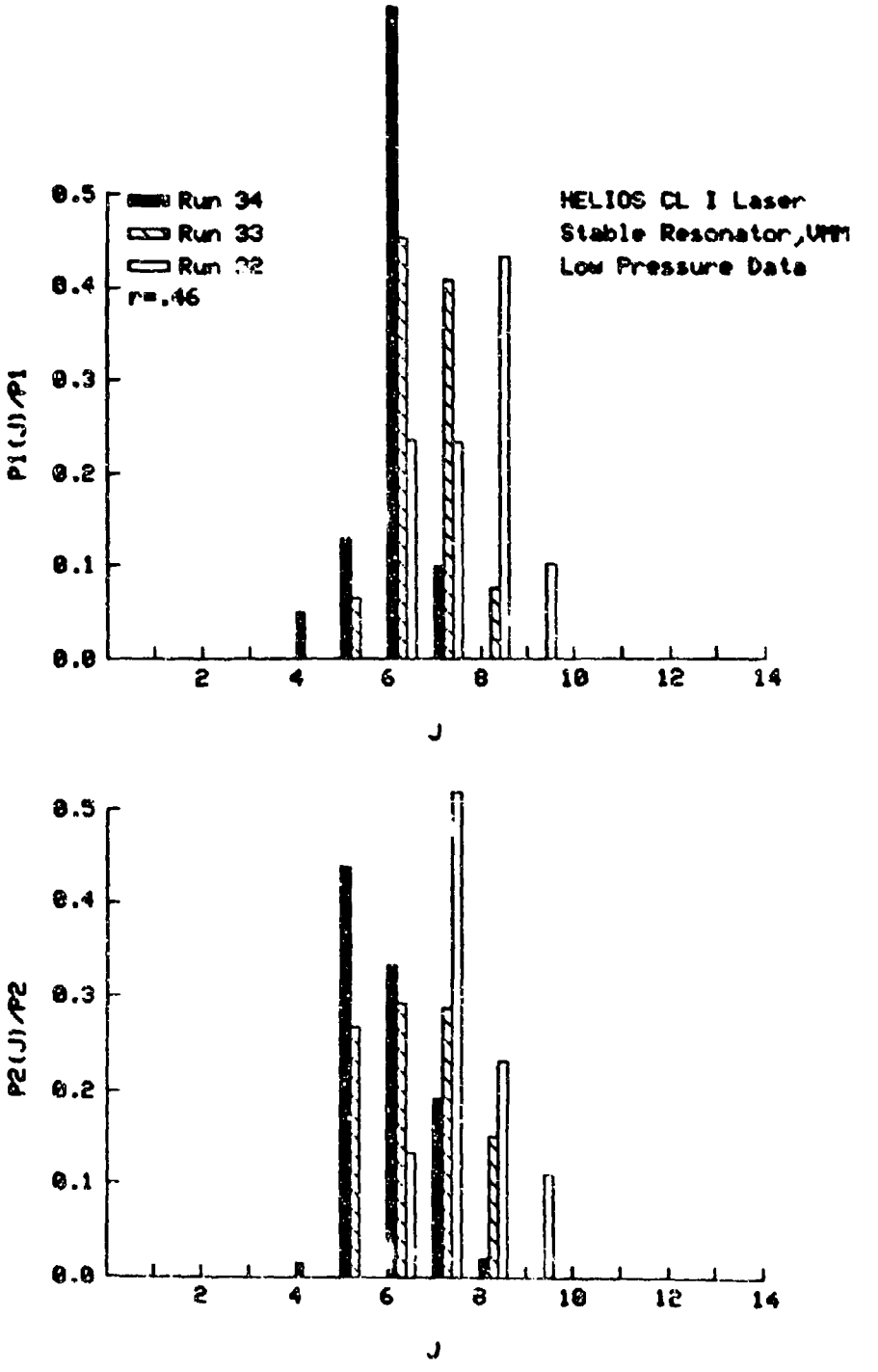

Figure 2. Experimental low pressure stable resonator power spectral distributions for the Helios CL I laser for three different SF_6 flow rates. $\dot{m}_{He}$ = 0.04.7 gm/sec, $\dot{m}_{O_2}$ = 0.147 gm/sec and $\dot{m}_{H_2}$ = 0.0228 gm/sec. A 46% reflective outcoupler was used in vacuum mirror mounts (VMM).

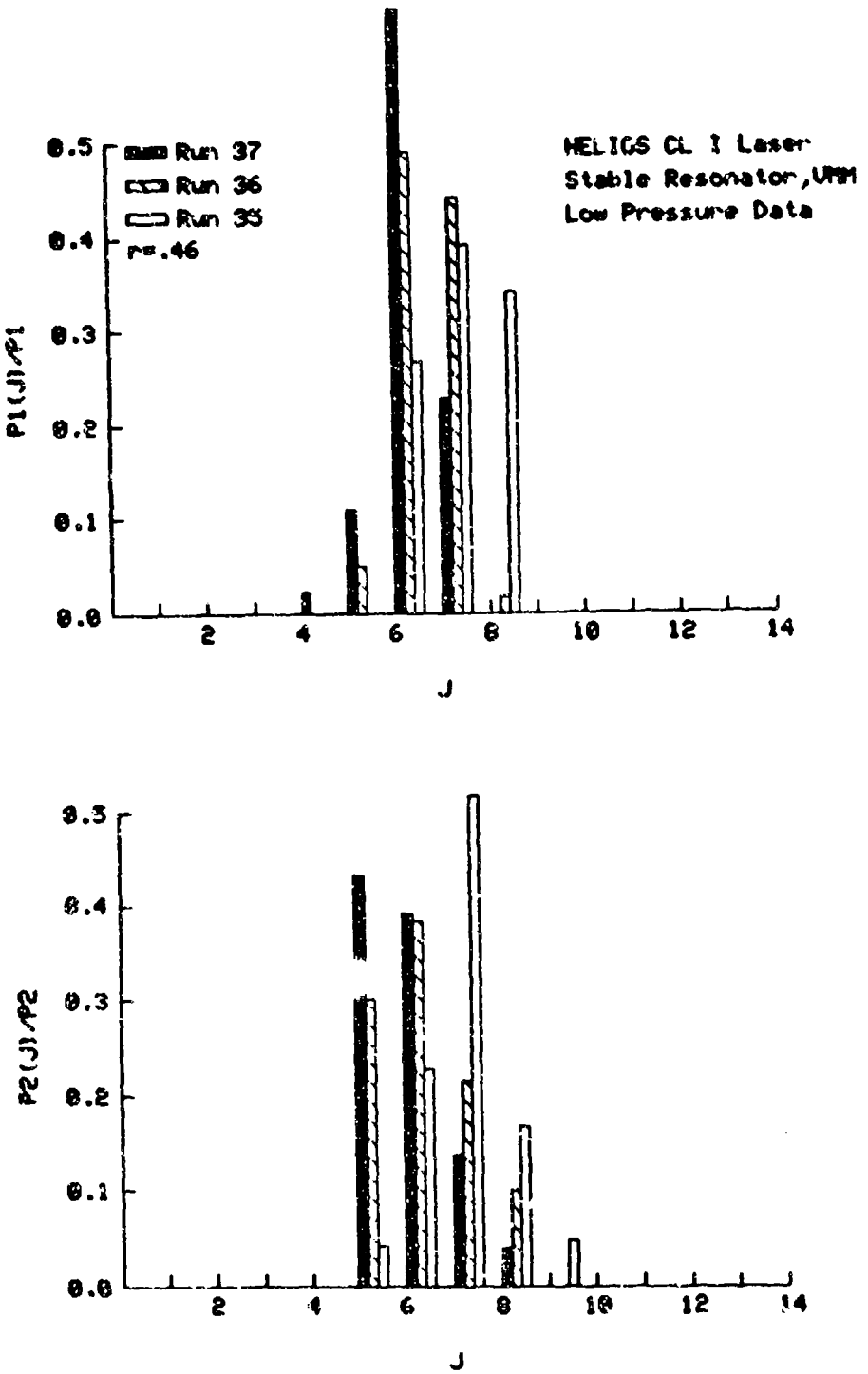

Figure 3. Experimental low pressure stable resonator power spectral distributions for the Helios CL I laser for three different SF_6 flow rates. $\dot{m}_{He}$ = 0.04[illegible] gm/sec, $\dot{m}_{O_2}$ = 0.147 gm/sec and $\dot{m}_{H_2}$ = 0.0305 gm/sec. A 46% reflective outcoupler was used in VMM.

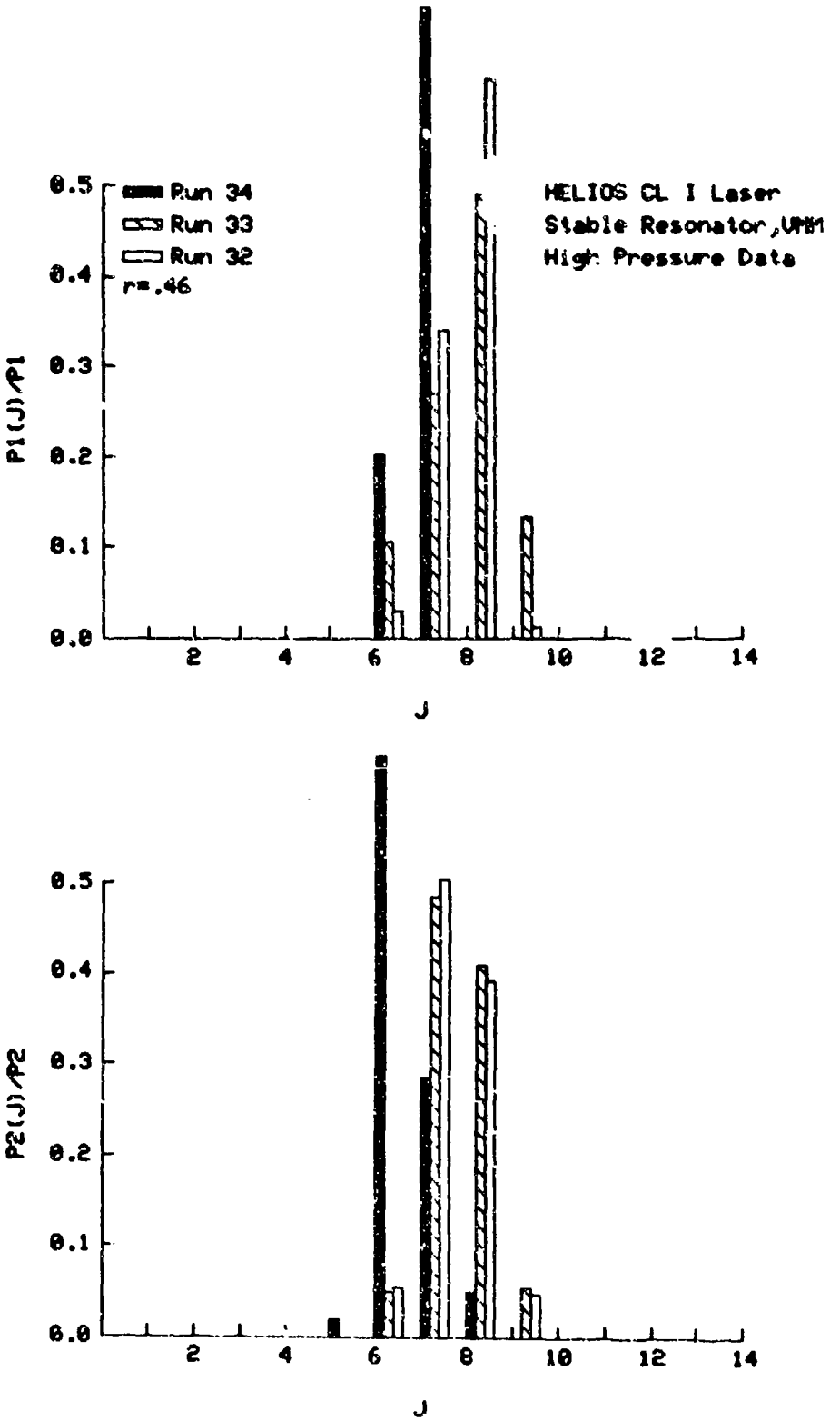

Figure 4. Experimental high pressure stable resonator power spectral distributions for the Helios CL I laser for three different SF_6 flow rates. $\dot{m}_{H_2}$ = 0.0437 gm/sec, $\dot{m}_{O_2}$ = 0.147 gm/sec and $\dot{m}_{H_2}$ = 0.0228 gm/sec. A 46% reflective outcoupler was used in VMM.

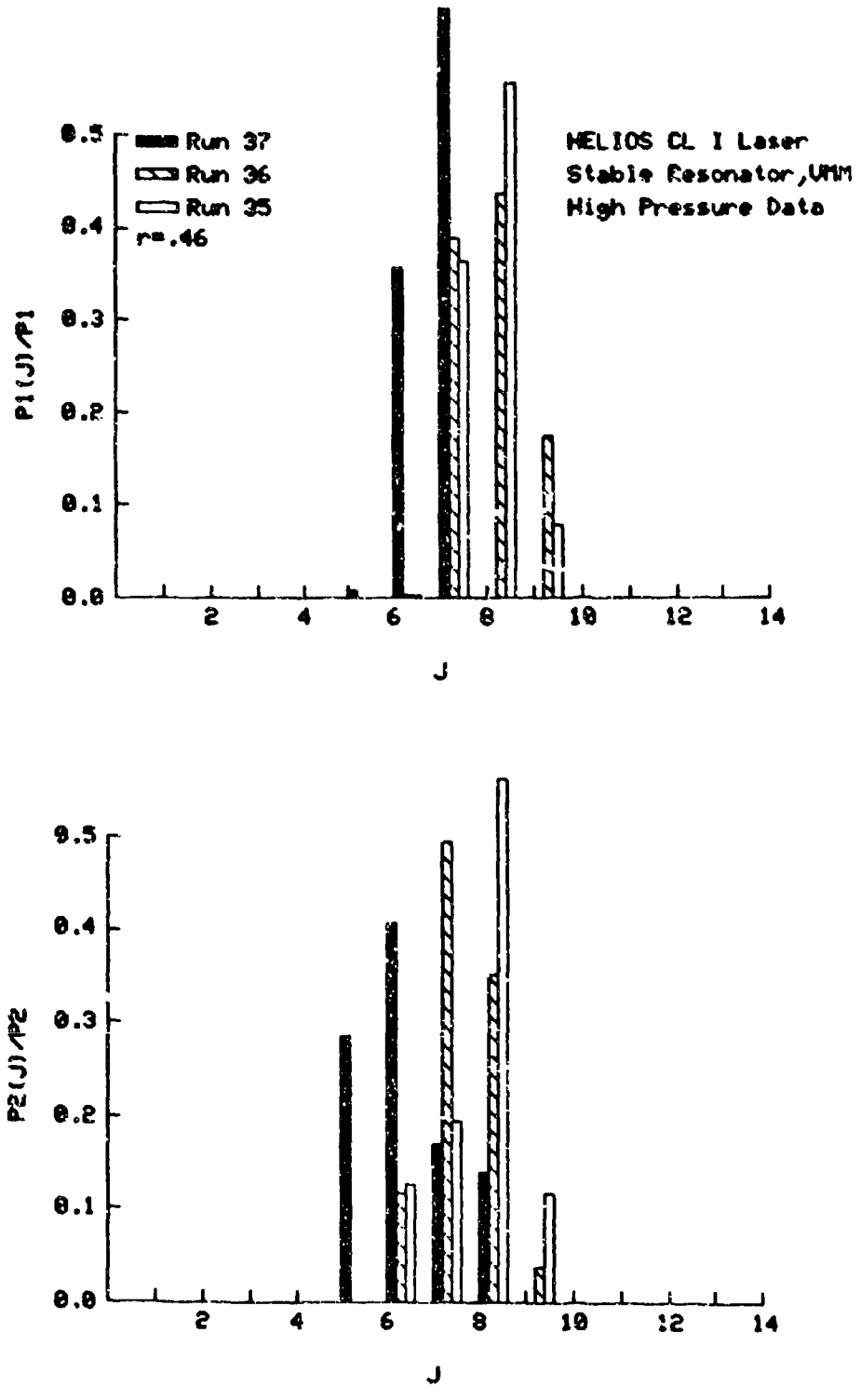

Figure 5. Experimental high pressure stable resonator power spectral distributions for the Helios CL I laser for three different SF_6 flow rates. $\dot{m}_{He}$ = 0.0437 gm/sec, $\dot{m}_{O_2}$ = 0.147 gm/sec and $\dot{m}_{H_2}$ = 0.0305 gm/sec. A 46% reflective outcoupler was used in VMM.

2.1.3 STABLE RESONATOR IN EXTERNAL MIRROR MOUNTS, $r_{eff} = 0.34$

The resonator used the 46% partially reflective outcoupler and the 2 meter radii of curvature ETR, but in this configuration the mirrors are mounted externally. These external mirror mounts (EMM) are rigidly held together by an invar rod structure which is placed on two translation stages to allow movement of the optical axis in the upstream-downstream direction. The distance between the mirrors was 1 meter with the CL I laser body centered between them. All the data were taken at the x_c (location of the optical axis) that gave maximum power, since the data will be compared with the VMM data which was always taken at the x_c for peak power.

To seal the laser cavity, two 4 cm CaF_2 Brewster windows were attached to the laser body. These Brewster windows were new and hence their loss had to be determined. By using the same procedure as outlined in Reference 1, it was determined that the new Brewster windows induce a 12% loss. Thus, when using the 46% reflective outcoupler and the new Brewster windows, the effective cavity reflectivity was 34%.

The peak power, fraction of the power in the 1→0 vibrational band and the beam diameter for the six combinations of SF_6 and H_2 flow rates for the low and high pressure cases are summarized in Tables 3 and 4, respectively. The power spectral distributions for these twelve cases are presented in Figures 6 through 9. The same spectral trends are observed in the EMM data as in the VMM data, that is, the spectra shift toward higher J lines as the SF_6 flow rate increased and, for a fixed flow rate, the power spectral distribution shifted toward higher J lines as pressure increased.

2.1.4 COMPARISON OF CL I AND CL II PERFORMANCE FOR THE SAME CAVITY LOSS

Summaries of the CL I and CL II stable resonator performance as a function of cavity loss and pressure are shown in Figures 10 through 13.

r_{eff} = 0.34, Low P

RUN NO.	32	33	34	35	36	37
$\dot{m}_{H_2}$ (gm/sec)	0.0228	0.0228	0.0228	0.0305	0.0305	0.0305
$\dot{m}_{SF_6}$ (gm/sec)	0.715	0.535	0.355	0.715	0.535	0.355
Blaze II (Input Data)						
% SF_6 Dissoc.	3.3	4.0	4.0	3.3	4.0	4.0
Initial T (°K)	500	450	450	500	450	450
H_2 Mixing Length	3.0	3.5	4.0	3.0	3.5	4.0
P (Meas.) (Torr)	6.7	6.0	5.4	7.2	6.5	5.8
P_T (Watts)						
Data	19.9	13.4	9.6	22.4	14.7	10.1
Blaze II	18.7	18.2	12.1	20.5	19.7	13.0
P_{10}/P_T						
Data	0.506	0.457	0.439	0.528	0.476	0.404
Blaze II	0.498	0.481	0.466	0.497	0.481	0.469
Beam Dia. (mm)						
Data	3.12	3.08	3.09	3.06	3.04	2.99
Blaze II	4.50	4.73	5.19	3.58	3.94	4.22

Table 3. Summary of the low pressure stable resonator data and Blaze II results for the Helios CL I with a 46% reflective outcoupler in EM[illegible] and 4 cm CaF_2 Brewster windows which result in a 34% effective reflectivity.

r_{eff} = 0.34, High P

RUN NO.	32	33	34	35	36	37
$\dot{m}_{H_2}$ (gm/sec)	0.0228	0.0228	0.0228	0.03	0.0305	0.0305
$\dot{m}_{SF_6}$ (gm/sec)	0.715	0.535	0.355	0.715	0.535	0.355
Blaze II (Input Data)						
% SF_6 Dissoc.	3.3	4.0	4.0	3.3	4.0	4.0
Initial T (°K)	500	450	450	500	450	450
H_2 Mixing Length	3.0	3.5	4.0	3.0	3.5	4.0
P (Meas.) (Torr)	11.5	10.7	10.0	12.3	11.6	10.7
P_T (Watts)						
Data	13.7	11.8	7.1	15.8	13.0	7.7
Blaze II	13.7	14.2	11.1	16.0	16.2	12.3
P_{10}/P_T						
Data	0.567	0.550	0.506	0.562	0.573	0.482
Blaze II	0.543	0.514	0.492	0.531	0.509	0.491
Beam Dia. (mm)						
Data	2.77	2.88	2.51	2.89	2.74	2.50
Blaze II	2.86	3.06	3.13	2.41	2.48	2.54

Table 4. Summary of the high pressure stable resonator data and Blaze II results for the Helios CL I with a 46% reflective outcoupler in EMM and 4 cm CaF_2 Brewster windows which result in a 34% effective reflectivity.

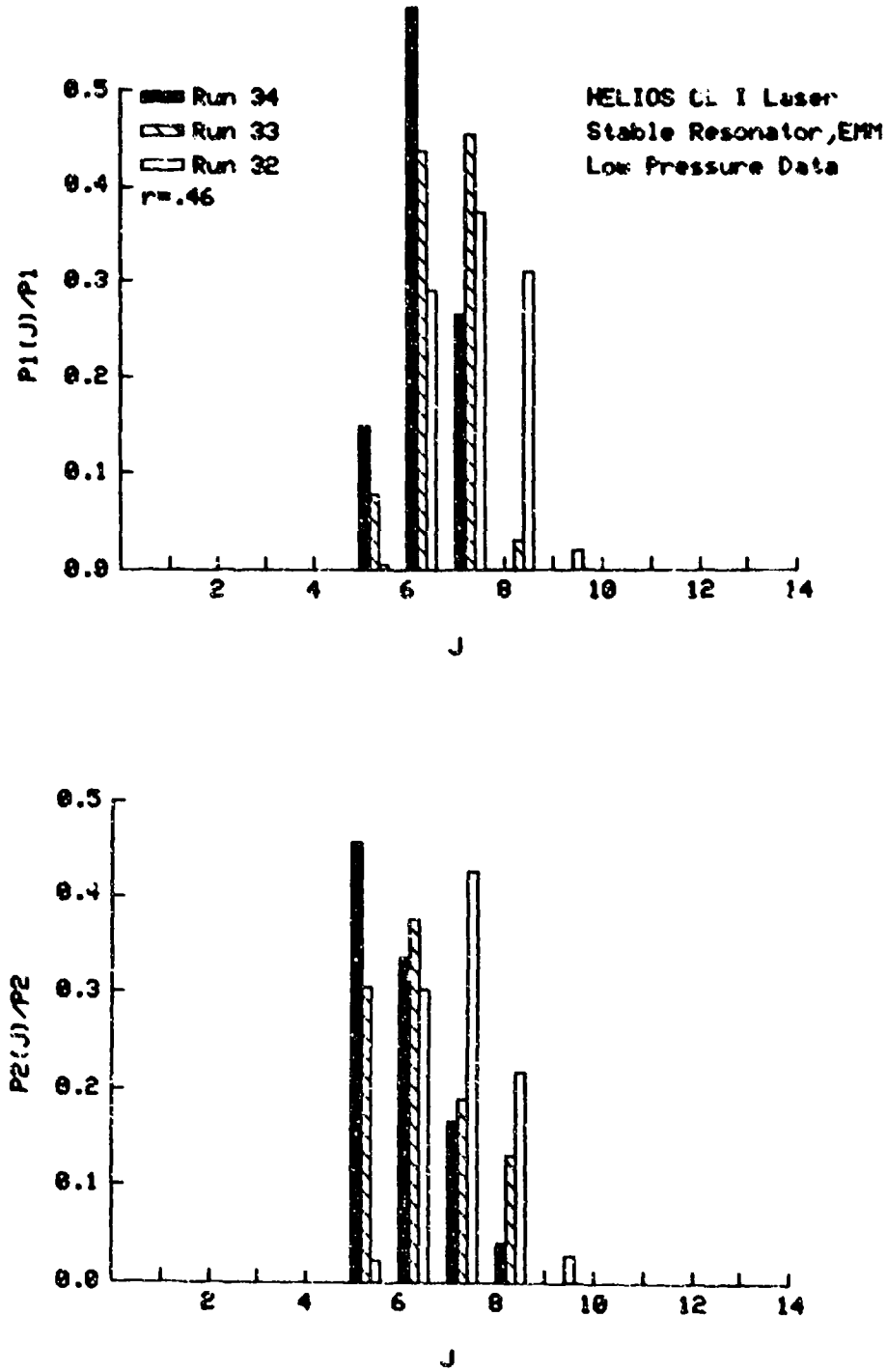

Figure 6. Experimental low pressure stable resonator power spectral distributions for the Helios CL 1 laser for three different SF_6 flow rates. $\dot{m}_{He}$ = 0.0437 gm/sec, $\dot{m}_{O_2}$ = 0.147 gm/sec and $\dot{m}_{H_2}$ = 0.0228 gm/sec. A 46% reflective outcoupler was used with external mirror mounts (EMM) and new 4 cm CaF_2 Brewster windows which result in a 34% effective reflectivity.

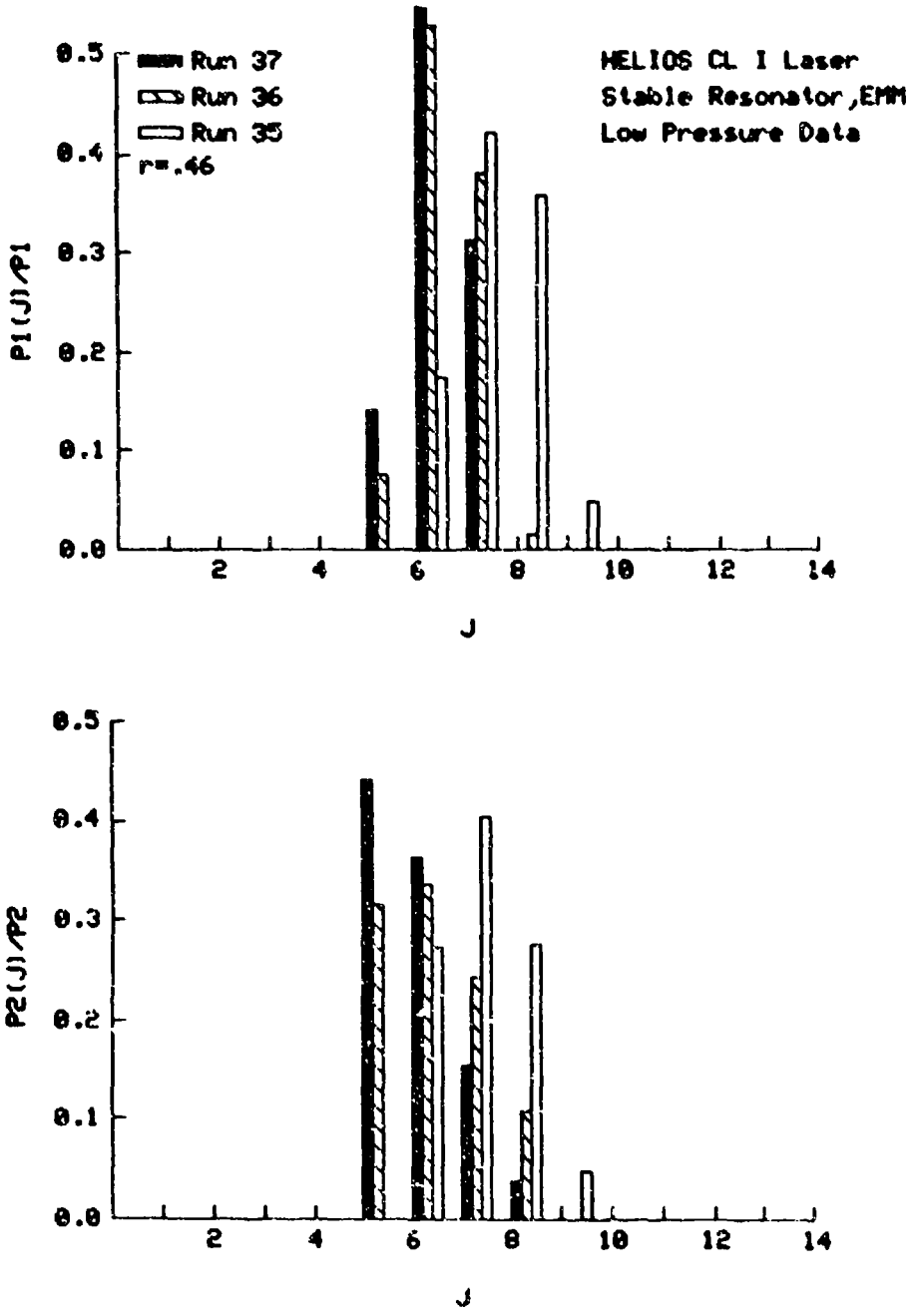

Figure 7. Experimental ow pre:ure stable resonator power spectral distributions for the Helios CL I laser for three different SF_6 flow rates. $\dot{m}_{He}$ = C.0437 gm/sec, $\dot{m}_{O_2}$ = 0.147 gm/sec and $\dot{m}_{H_2}$ =0.0305 gm/sec. A 46% reflective outcoupler was used with EMM and new 4 cm CaF_2 Brewster windows which result in a 34% effective reflectivity.

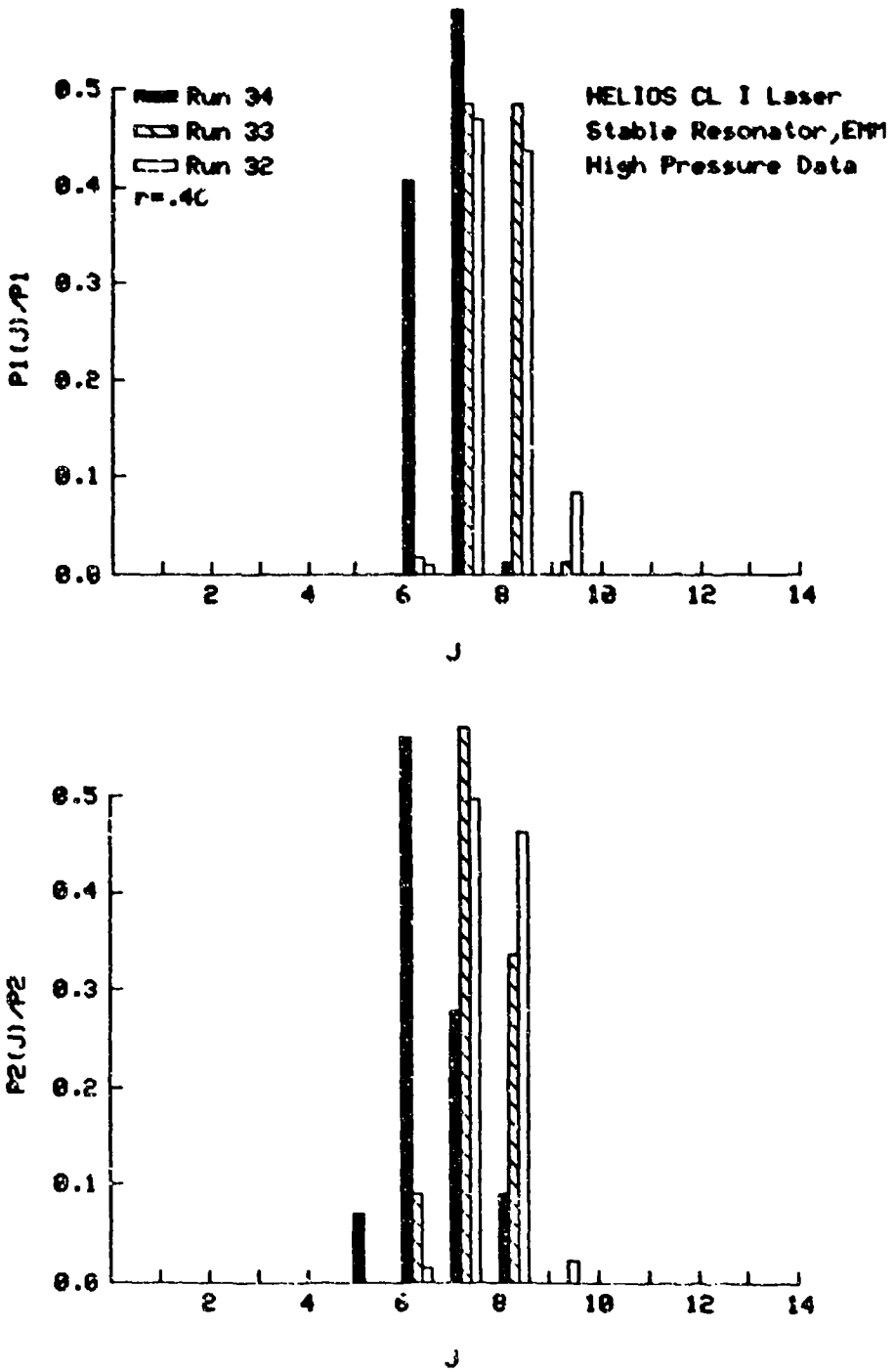

Figure 8. Experimental high pressure stable resonator power spectral distributions for the Helios CL I laser for three different SF_6 flow rates. $\dot{m}_{He}$ = 0.0437 gm/sec, $\dot{m}_{O_2}$ = 0.147 gm/sec and $\dot{m}_{H_2}$ = 0.0228 gm/sec. A 46% reflective outcoupler was used with EMM and new 4 cm CaF_2 Brewster windows which result in a 34% effective reflectivity.

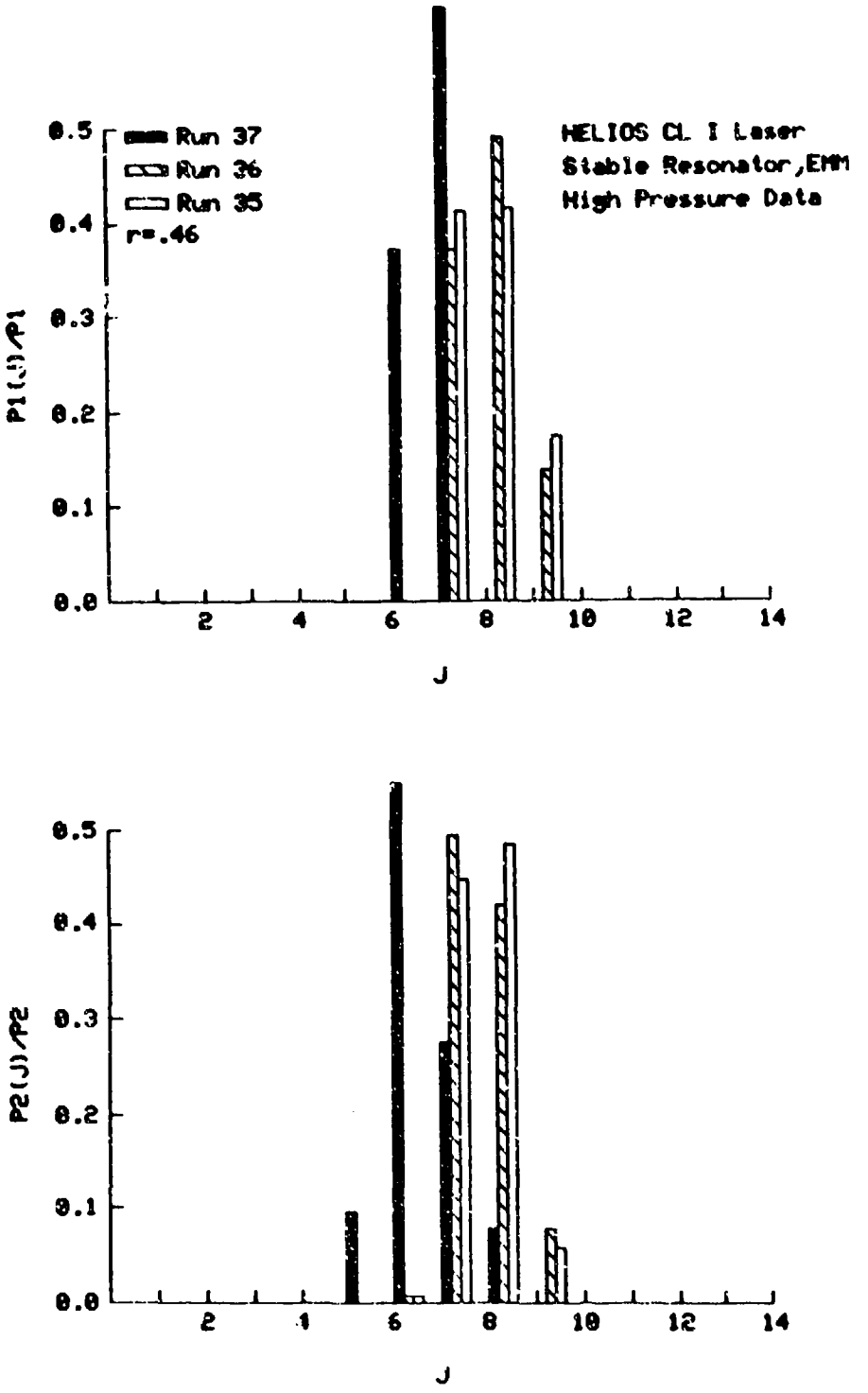

Figure 9. Experimental high pressure stable resonator power spectral distributions for the Helios CL I laser for three different SF_6 flow rates. $\dot{m}_{He}$ = 0.0437 gm/sec, $\dot{m}_{O_2}$ = 0.147 gm/sec and $\dot{m}_{H_2}$ = 0.0305 gm/sec. A 46% reflective outcoupler was used with EMM and new 4 cm CaF_2 Brewster windows which result in a 34% effective reflectivity.

Comparison of Figures 10 and 12 shows that the slopes of the power versus reflectivity curves are steeper for the CL II than for the CL I, except for the high pressure, highest SF_6 flow rates. For an effective reflectivity of 46%, for both high and low pressures, the CL I powers range from 38% to 54% of the CL II powers for the same cavity loss; 38-40% for Runs 34 and 37 (the lowest SF_6 flow rate), 39-48% for Runs 33 and 36 (the middle SF_6 flow rate), and 48-54% for Runs 32 and 35 (the highest SF_6 flow rate). Overall, the CL I power is an average of 45% of the CL II power for the same cavity loss independent of pressure, Table 5.

Comparison of the power spectral distributions of the CL I and the CL II for the same cavity loss showed a shift of the CL I spectral peak to one lower J, Figures 7 and 14. The lower J lines, $P_1(4)$ and $P_2(4)$, were present in the CL I low pressure, low SF_6 flow rates, $r_{eff} = 0.46$ spectra, Figures 2 and 3. These lines were not seen in the CL II spectra[1-5]. The occurrance of low J lines is accompanied by the loss of higher J Lines in the CL I spectra. In addition, there are fewer lines in the CL I spectra than in the CL II spectra. These effects can be explained by the fact that for the same cavity loss, the saturated gain in the CL I is twice as large as that in the CL II. This is seen from the equation

$$\alpha_{sat} = -\frac{1}{2L_e} \ln r_o r_L \qquad (2.1.4\text{-}1)$$

where α_{sat} is the saturated gain, L_e is the thickness of the mixed flow and r_o and r_L are the mirror reflectivities[6]. For the same cavity loss, r_o and r_L are the same for both the CL I and CL II; however, $L_{e_{CL\ II}} = 2\, L_{e_{CL\ I}}$ and thus

$$\alpha_{sat_{CL\ I}} = 2\alpha_{sat_{CL\ II}} \qquad (2.1.4\text{-}2)$$

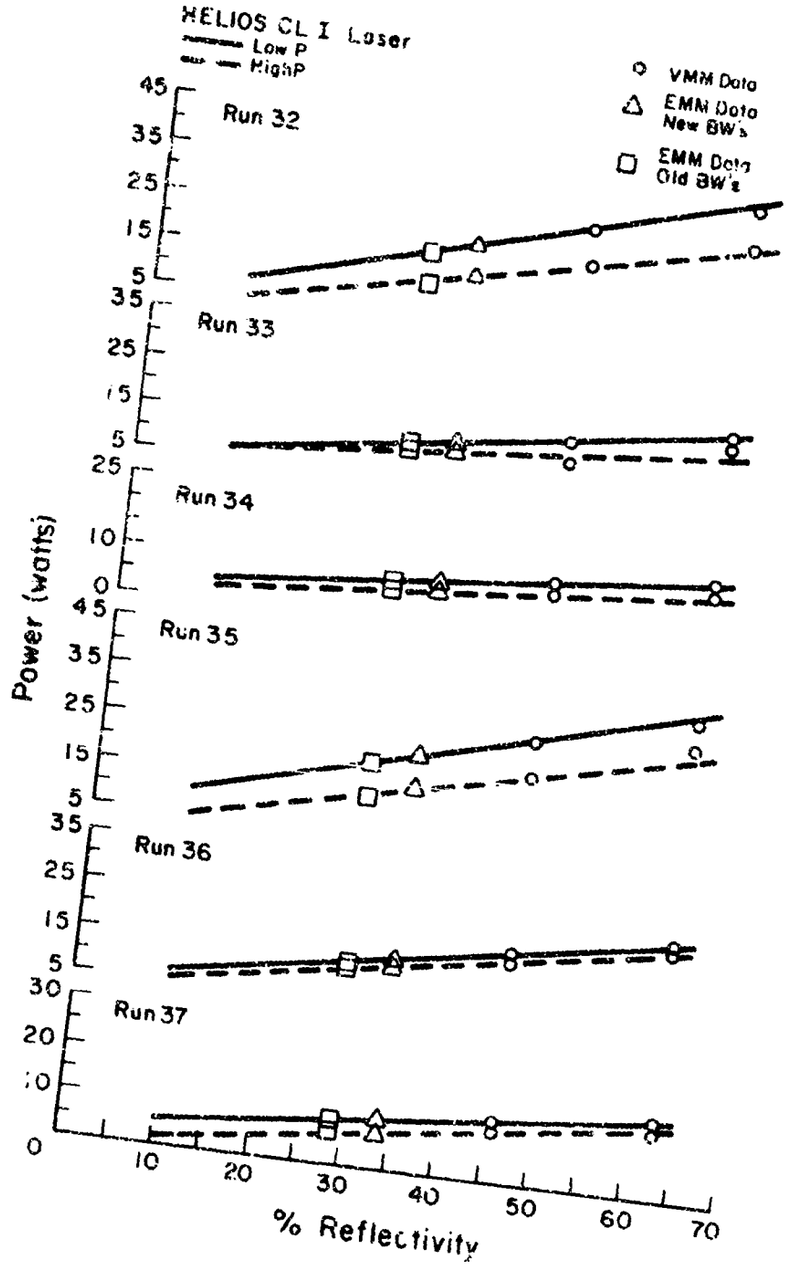

Figure 10. Experimental Helios CL I stable resonator total power versus % reflectivity for low and high pressure. The EMM data has been plotted assuming that the loss introduced by the new Brewster windows was 12%. The old Brewster windows introduced a 17% loss.

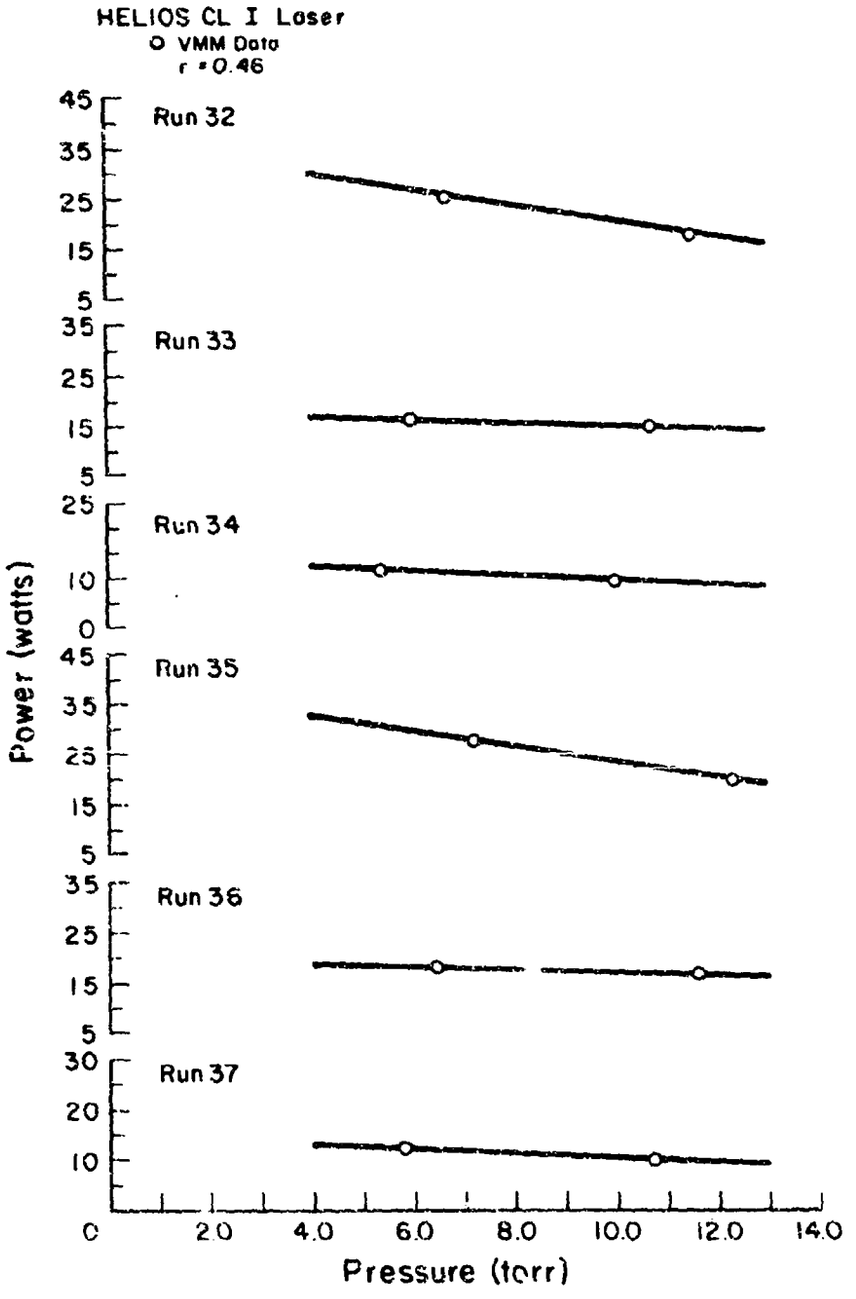

Figure 11. Experimental Helios CL I stable resonator total power versus cavity pressure for VMM with a cavity reflectivity of 46%.

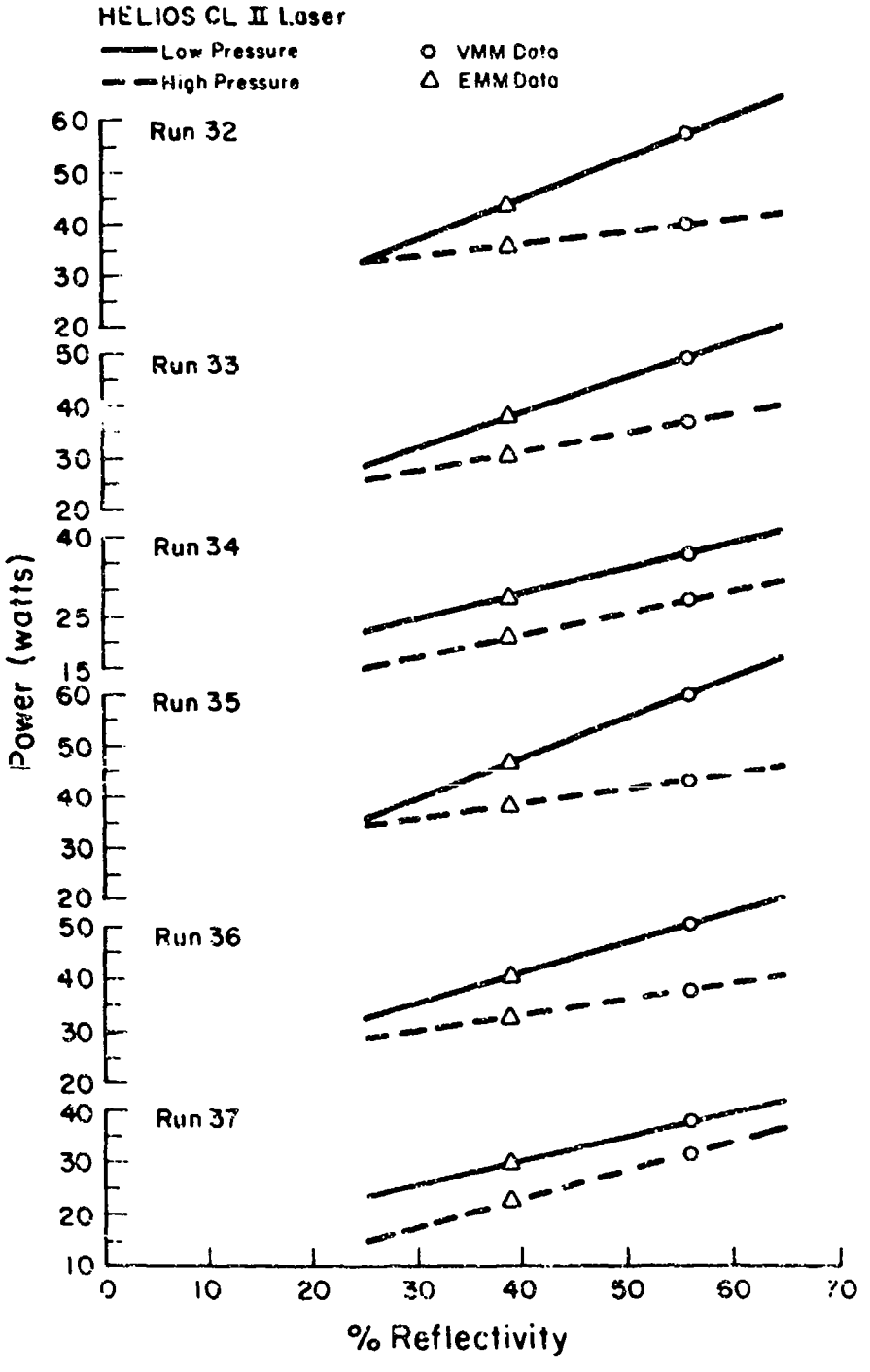

Figure 12. Experimental Helios CL II stable resonator total power versus % reflectivity for low and high pressure.[4] The EMM data has been plotted assuming that the loss introduced by the old Brewster wind ws was 17%.

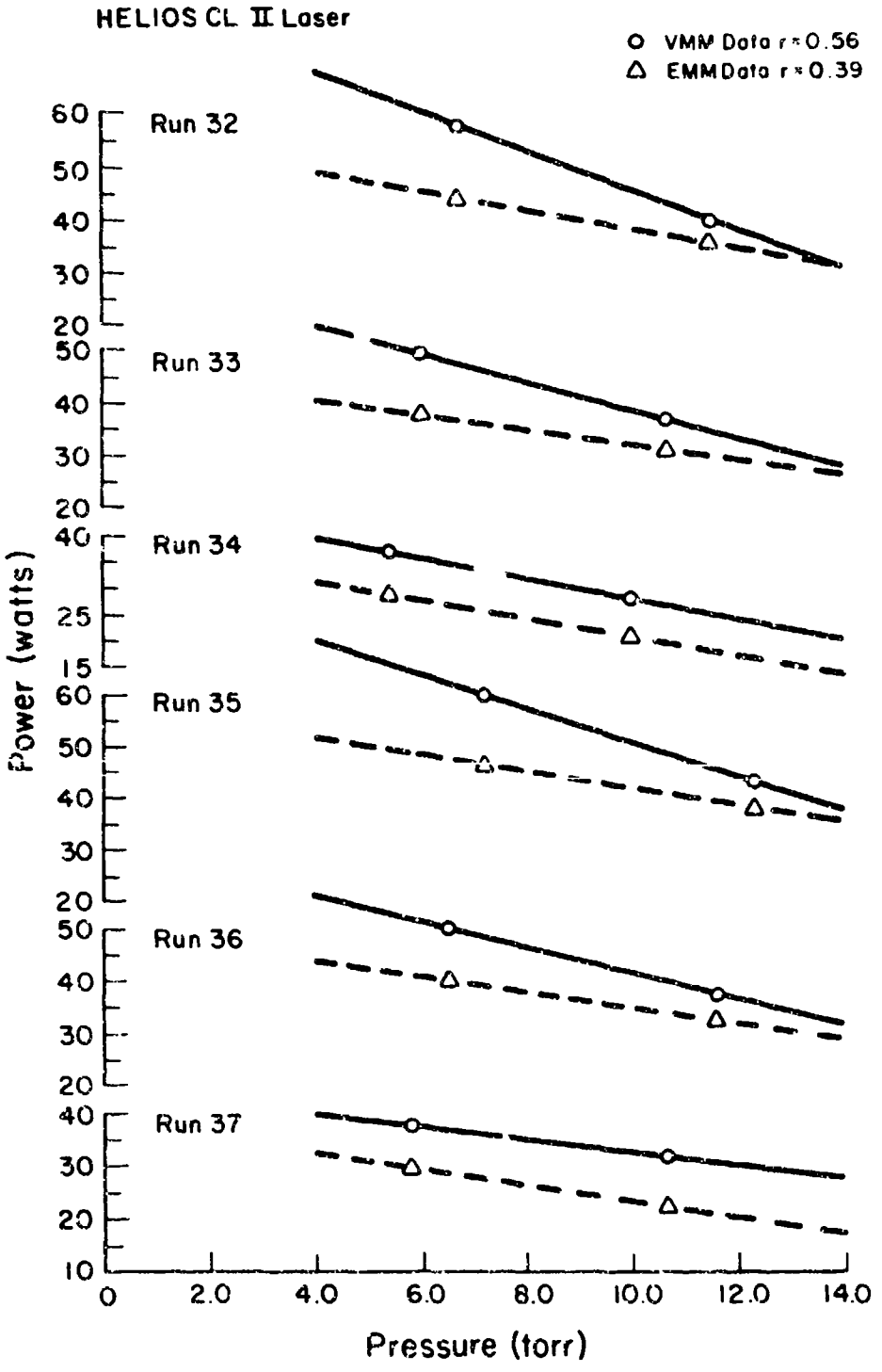

Figure 13. Experimental Helios CL II stable resonator total power versus pressure for two optical configurations.[4] The VMM cavity reflectivity was 56% and EMM effective cavity reflectivity was 39%.

CL I Data, r_{eff} = 0.46

RUN NO.	32	33	34	35	36	37
Low Pressure						
CL I	25.4	16.7	11.7	28.0	18.2	12.6
CL II	49.1	42.2	30.6	51.7	44.2	32.8
% (CL I/CL II)	51.7	39.6	38.2	54.2	41.2	38.4
High Pressure						
CL I	17.8	15.0	9.0	20.0	16.7	10.3
CL II	37.0	32.8	23.3	40.0	34.7	25.9
% (CL I/CL II)	48.1	45.7	38.6	50.0	48.1	39.8

Overall Average % (CL I/CL II) = 44.5

Table 5. Comparison of the Helios CL I and CL II stable resonator total power data when the cavity losses are the same for low and high pressure.

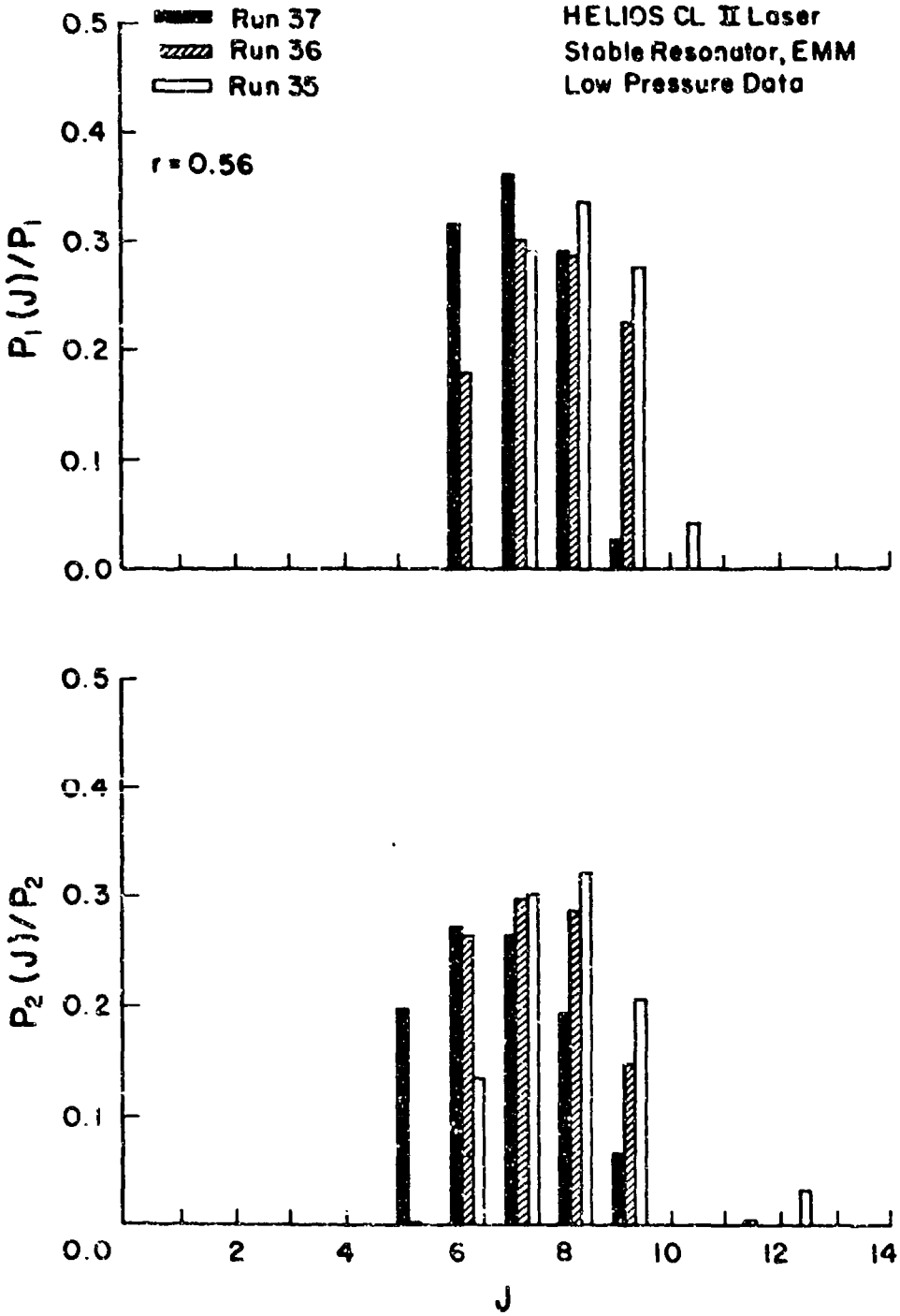

Figure 14. Experimental low pressure stable resonator power spectral distributions for the Helios CL II laser for three different SF_6 flow rates.[4] $\dot{m}_{He}$ = 0.0874 gm/sec, $\dot{m}_{O_2}$ = 0.294 gm/sec and $\dot{m}_{H_2}$ = 0.0610 gm/sec. A 56% reflective outcoupler was used with EMM and old 4 cm CaF_2 Brewster windows which result in a 39% effective reflectivity.

Since the CL I has a higher saturated gain, fewer lines will lase. When there are fewer lines, the stronger spectral lines are more pronounced as seen in all of the CL I spectra (i.e., $P_1(J)/P_1$ exceeds 0.50 and in some cases 0.70).

Comparison of the beam diameters of the two lasers for the same cavity loss shows that the beam diameters of the CL I are smaller than those of the CL II, Table 6. For the low pressure cases it is seen that the CL I beam diameters are from 1.78 to 2.01 mm smaller for the low H_2 flow rates and from 1.46 to 1.54 mm smaller for the high H_2 flow rates. For the high pressure cases, the CL I beam diameters are from 0.39 to 1.27 mm smaller for all flow rates, except for one case, Run 37, where the CL I beam diameter is actually 0.25 mm larger. The smaller beam diameters exhibited by the CL I laser are a consequence of the higher saturated gain of the CL I. Figure 15 shows how increased saturated gain causes the beam diameter of an individual line to be smaller for the CL I laser. This is true for all lines and thus the CL I laser has smaller beam diameters than the CL II laser. It should be noted that this comparison was made for both lasers in EMM configuration.

2.1.5 STABLE RESONATOR IN VMM, $r_{eff} = 0.63$

The resonator consisted of a 3% partially reflective outcoupler and the ETR in VMM as described in Section 2.1.2. With this resonator, the saturated gain in the CL I was the same as the saturated gain in the CL II when the effective reflectivity of the CL II resonator was 39%. These data were taken to provide information on the scale effects of changing the size of a laser while keeping the saturated gain the same.

The peak power, fraction of the power in the 1-0 vibrational band and beam diameter for the six combinations of SF_6 and H_2 flow rates, for the low and high pressure cases, are summarized in Tables 7 and 8, respectively. The power spectral distributions for these twelve cases are presented in Figures

Case	RUN NO. 32	33	34	35	36	37
Beam Diameters, Low Pressure						
CL I, r_{eff} = 0.34	3.12	3.08	3.09	3.06	3.04	2.99
CL II, r_{eff} = 0.39	4.90	5.00	5.10	4.60	4.50	4.50
Beam Diameters, High Pressure						
CL I, r_{eff} = 0.34	2.77	2.88	2.51	2.89	2.74	2.50
CL II, r_{eff} = 0.39	3.39	3.43	2.91	3.21	3.06	3.09
CL I, r_{eff} = 0.46	2.08	2.36	1.62	2.22	2.47	3.02
CL II, r_{eff} = 0.43	2.92	3.03	2.89	2.84	2.86	2.77

Table 6. Comparison of the Helios CL I and CL II[1,4] stable resonator beam diameters with almost the same cavity loss for low and high pressure.

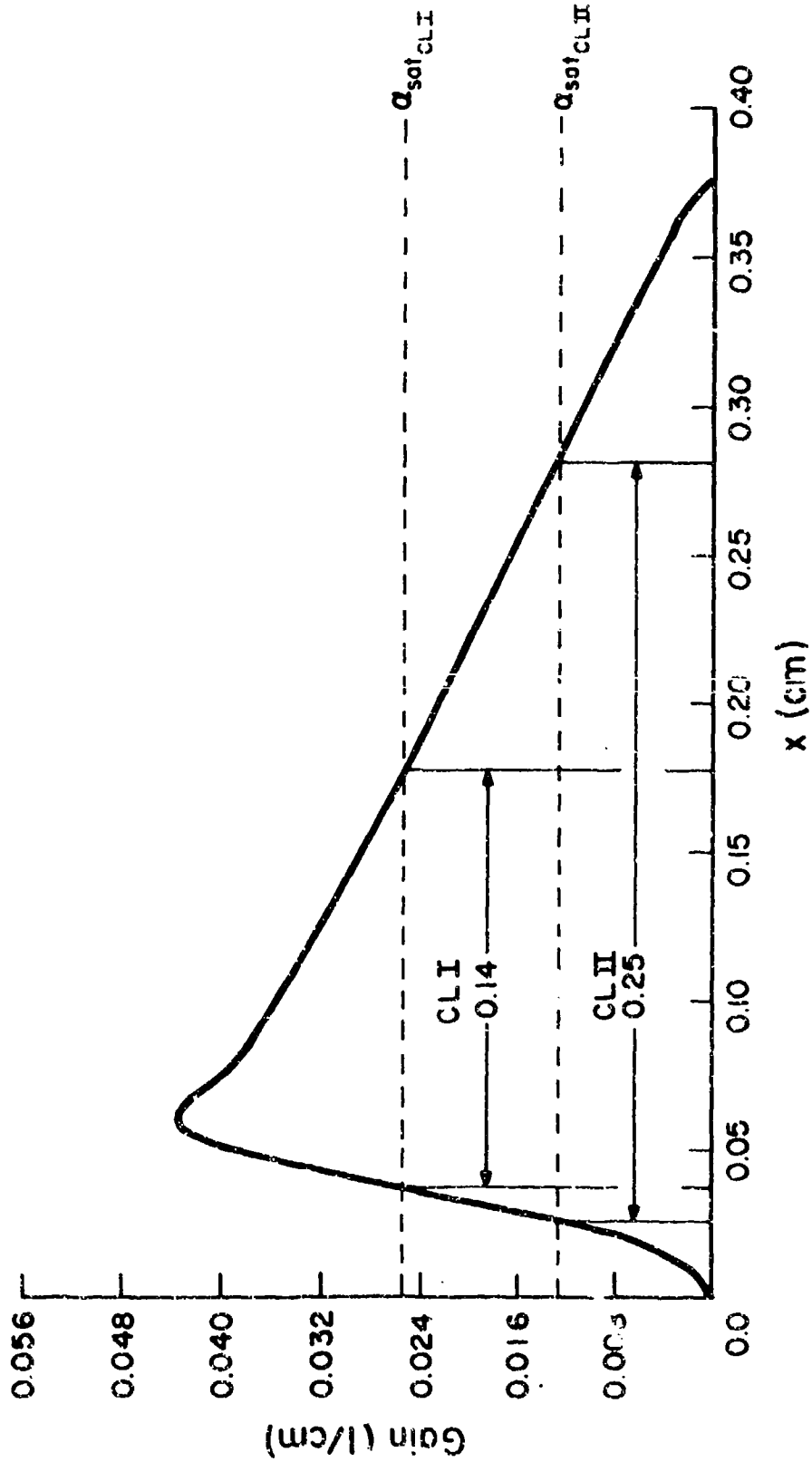

Figure 15. A typical P-branch zero power gain curve for the 2 → 1 vibrational band for J = 5. This diagram shows how increased saturated gain causes the CL I beam diameters to be smaller than the CL II beam diameters.

r_{eff} = 0.63, Low P

RUN NO.	32	33	34	35	36	37
$\dot{m}_{H_2}$ (gm/sec)	0.0228	0.0228	0.0228	0.0305	0.0305	0.0305
$\dot{m}_{SF_6}$ (gm/sec)	0.715	0.535	0.355	0.715	0.535	0.355
Blaze II (Input Data)						
% SF_6 Dissoc.	3.3	4.0	4.0	3.3	4.0	4.0
Initial T (°K)	500	450	450	500	450	450
H_2 Mixing Length	3.0	3.5	4.0	3.0	3.5	4.0
P (Meas.) (Torr)	6.7	6.0	5.4	7.2	6.5	5.8
P_T (Watts)						
Data	33.2	21.6	15.3	35.7	23.0	15.5
Blaze II	26.7	25.5	17.5	28.1	26.8	18.3
P_{10}/P_T						
Data	0.706	0.434	0.347	0.589	0.423	0.568
Blaze II	0.502	0.492	0.486	0.502	0.493	0.485
Beam Dia. (mm)						
Data	3.60	3.03	3.45	2.70	2.46	3.00
Blaze II	4.82	5.24	5.46	3.80	4.18	4.40

Table 7. Summary of the low pressure stable resonator data and Blaze II results for the Helios CL I with a 63% reflective outcoupler in VMM.

r_{eff} = 0.63, High P

RUN NO.	32	33	34	35	36	37
$\dot{m}_{H_2}$ (gm/sec)	0.0228	0.0228	0.0228	0.0305	0.0305	0.0305
$\dot{m}_{SF_6}$ (gm/sec)	0.715	0.535	0.355	0.715	0.535	0.355
Blaze II (Input Data)						
% SF_6 Dissoc.	3.3	4.0	4.0	3.3	4.0	4.0
Initial T °(K)	500	450	450	500	450	450
H_2 Mixing Length	3.0	3.5	4.0	3.0	3.5	4.0
P (Meas.) (Torr)	11.5	10.7	10.0	12.3	11.6	10.7
P_T(Watts)						
Data	25.0	19.2	13.1	30.3	22.0	14.0
Blaze II	20.9	20.8	15.9	23.1	22.6	17.0
P_{10}/P_T						
Data	0.446	0.635	0.500	0.470	0.549	0.440
Blaze II	0.529	0.511	0.499	0.523	0.509	0.498
Beam Dia. (mm)						
Data	2.91	2.38	2.76	2.51	2.41	2.33
Blaze II	3.26	3.37	3.36	2.63	2.48	2.70

Table 8. Summary of the high pressure stable resonator data and Blaze II results for the Helios CL I with a 63% reflective outcoupler in VMM.

16 through 19. From these figures it is seen that the spectra shift toward higher J lines as the SF_6 flow rate increased and, for a fixed flow rate, the spectra shift toward higher J lines as pressure increased. The reasons for these shifts are detailed in Section 2.1.2. The appearance of the lines $P_2(10)$, $P_2(11)$ and $P_2(12)$ at the highest SF_6 flow rates should be noted. When the saturated gain in the CL I is the same as in the CL II, the minimum in the spectra at $P_2(11)$ is observed in the CL I as it was in the CL II[1,2,4]. This minimum at $P_2(11)$ can be explained by collisional effects[1,2,4]. It is believed that this minimum is caused by a near resonant energy transfer from v=3, J=3, 4 to v=2, J=14 with a subsequent rotational cascade to v=2, J=11, which is the upper level for the $P_2(12)$ line. This line lases and thus blocks the rotational cascade to v=2, J=10, which is the upper level for the $P_2(11)$ line which causes the $P_2(11)$ line to be weaker than the $P_2(12)$ line. At higher pressure, this effect becomes more pronounced due to the increased collision frequency and thus the collisional energy transfer is more important, which explains why the minimum occurs at high pressure, but not at low pressure.

As noted in Section 2.1.4, when the losses in the CL I and the CL II were the same, the higher J lines, $P_2(10)$-$P_2(12)$, did not lase in the CL I because the saturated gain in the CL I was twice as large as in the CL II. Thus, the minimum at $P_2(11)$ was not observed in the CL I spectra. However, as noted above, when the saturated gain in the CL I was the same as in the CL II, the minimum at $P_2(11)$ was observed in the CL I spectra.

2.1.6 COMPARISON OF CL I AND CL II PERFORMANCE FOR THE SAME SATURATED GAIN

To compare the performance of the CL I and CL II lasers when the saturated gain in the two lasers was the same, the effective reflectivity of the laser cavities must be adjusted to give the same α_{sat}. From Eq. (2.1.4-1)

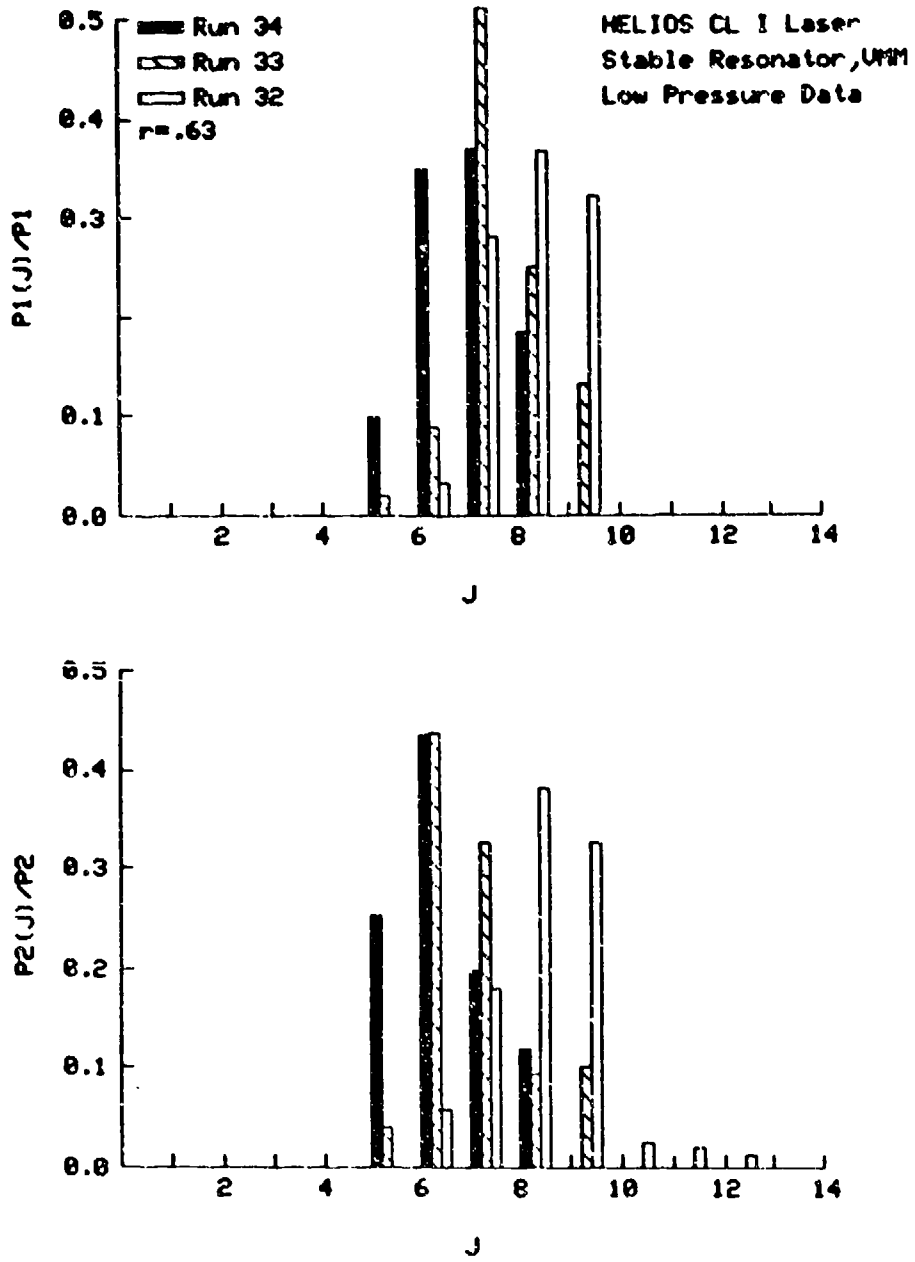

Figure 16. Experimental low pressure stable resonator power spectral distributions for the Helios CL I laser for three different SF_6 flow rates. $\dot{m}_{He}$ = 0.0437 gm/sec, $\dot{m}_{O_2}$ = 0.147 gm/ sec and $\dot{m}_{H_2}$ = 0.0228 gm/sec. A 63% reflective outcoupler was used in VMM.

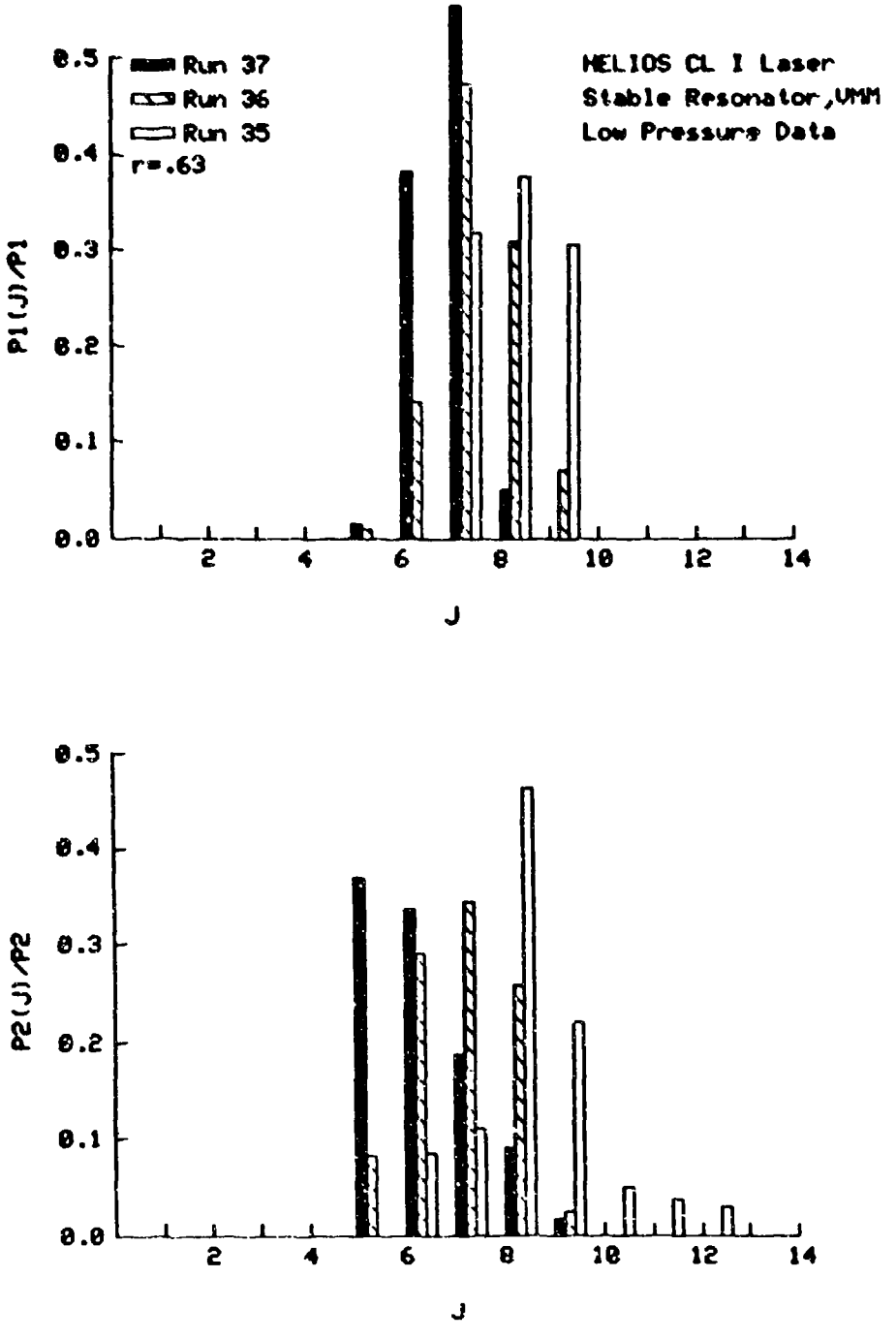

Figure 17. Experimental low pressure stable resonator power spectral distributions for the Helios CL I laser for three different SF_6 flow rates. $\dot{m}_{He}$ = 0.0437 gm/sec, $\dot{m}_{O_2}$ = 0.147 gm/sec and $\dot{m}_{H_2}$ = 0.0305 gm/sec. A 63% reflective outcoupler was used in VMM.

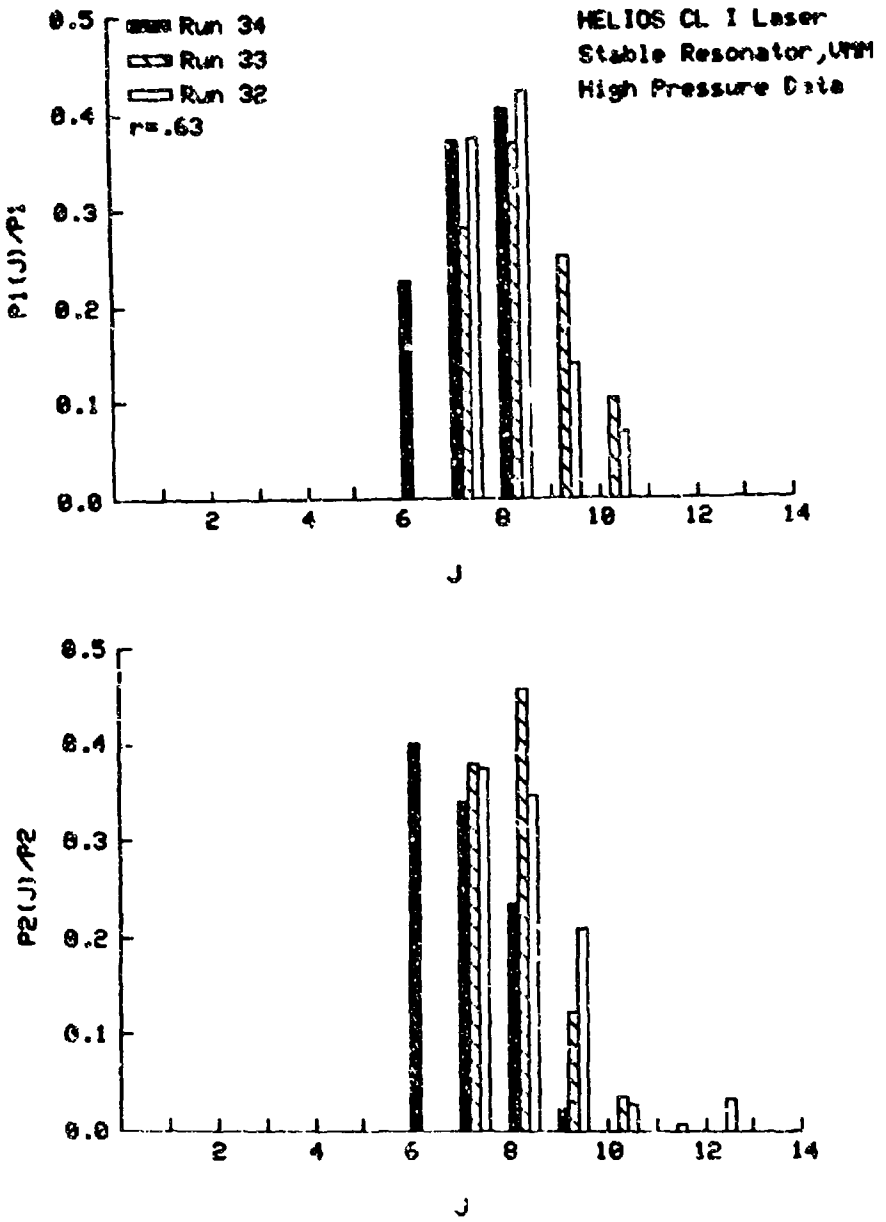

Figure 18. Experimental high pressure stable resonator power spectral distributions for the Helios CL I laser for three different SF_6 flow rates. $\dot{m}_{He}$ = 0.0437 gm/sec, $\dot{m}_{O_2}$ = 0.147 gm/sec and $\dot{m}_{H_2}$ = 0.0228 gm/sec. A 62% reflective outcoupler was used in VMM.

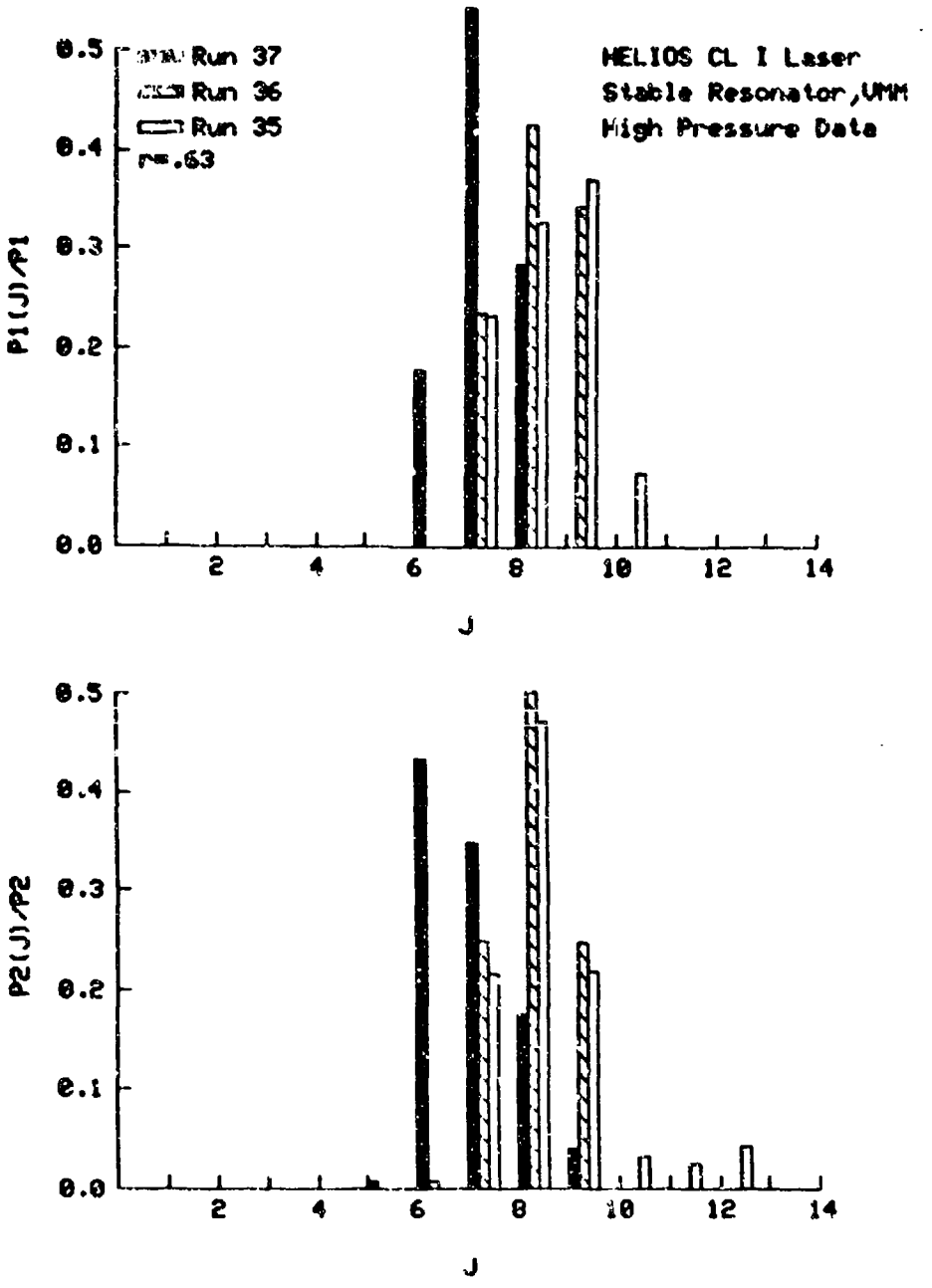

Figure 19. Experimental high pressure stable resonator power spectral distributions for the Helios CL I laser for three different SF_6 flow rates. $\dot{m}_{He}$ = 0.0437 gm/sec, $\dot{m}_{O_2}$ = 0.147 gm/sec and $\dot{m}_{O_2}$ = 0.0305 gm/sec A 63% reflective outcoupler was used in VMM.

$$\alpha_{sat_{CL\ I}} = -\frac{1}{2L_{e_{CL\ I}}} \ln r_{o_{CL\ I}} r_{L_{CL\ I}} \qquad (2.1.6\text{-}1)$$

$$\alpha_{sat_{CL\ II}} = -\frac{1}{2L_{e_{CL\ II}}} \ln r_{o_{CL\ II}} r_{L_{CL\ II}} \qquad (2.1.6\text{-}2)$$

For the two lasers used, $L_{e_{CL\ II}} = 2L_{e_{CL\ I}}$ and $r_{L_{CL\ I}} = r_{L_{CL\ II}}$. Thus, setting $\alpha_{sat_{CL\ I}} = \alpha_{sat_{CL\ II}}$ gives

$$\ln r_{o_{CL\ I}} r_{L_{CL\ I}} = \frac{1}{2} \ln r_{o_{CL\ II}} r_{L_{CL\ I}} \qquad (2.1.6\text{-}3)$$

Solution of this equation for the reflectivity of the CL II outcoupler gives

$$r_{o_{CL\ II}} = r^2_{o_{CL\ I}} r_{L_{CL\ I}} \qquad (2.1.6\text{-}4)$$

Therefore, when a 63% partially reflective outcoupler is used with the CL I ($r_{o_{CL\ I}} = 0.63$) along with the ETR ($r_{L_{CL\ I}} = 0.995$), the CL II laser will have the same saturated gain when $r_{o_{CL\ II}} = 0.39$ (i.e., the effective reflectivity of the CL II outcoupler must be 39%).

Comparison of the peak power data for the CL I and CL II[4] for the same saturated gain, Table 9, shows that, for low pressure the CL I powers range from 52-77% of the CL II powers; 52-54% for Runs 34 and 37 (the low SF_6 flow rate), 57-58% for Runs 33 and 36 (the middle SF_6 flow rate), and 76-77% for Runs 32 and 35 (the highest SF_6 flow rate). Overall, the CL I power is an average of 62% of the CL II power for low pressure. For high pressure, the CL I powers range from 63-80% of the CL II powers, Table 9; 63-68% for the low and middle SF_6 flow rates and 70-80% for the highest SF_6 flow rate. Overall, for high pressure, the CL I power is an average of 68% of the CL II power. Two differences between the comparison of the same cavity loss and the

RUN NO.	32	33	34	35	36	37
P_T (Watts)						
CL I, Low P	33.2	21.6	15.3	35.7	23.0	15.5
CL II, Low P	43.7	37.5	28.2	46.2	40.2	29.6
% (CL I/ CL II)	76.0	57.6	54.3	77.3	57.2	52.4
CL I, High P	25.0	19.2	13.1	30.3	22.0	14.0
CL II, High P	35.5	30.5	20.6	38.0	32.5	22.1
% (CL I/CL II)	70.4	63.0	63.6	79.7	67.7	63.3
P_{10}/P_T						
CL I, Low P	0.706	0.434	0.347	0.589	0.423	0.568
CL II, Low P	0.481	0.512	0.468	0.493	0.511	0.472
CL I, High P	0.446	0.635	0.500	0.470	0.549	0.440
CL II, High P	0.530	0.483	0.472	0.520	0.531	0.474
Beam Diameter (mm)						
CL I, Low P	3.60	3.03	3.45	2.70	2.46	3.00
CL II, Low P	4.90	5.00	5.10	4.60	4.50	4.50
CL I, High P	2.91	2.38	2.76	2.51	2.41	2.33
CL II, High P	3.39	3.43	2.91	3.21	3.06	3.09

Table 9. Comparison of the Helios CL I and CL II[4] low and high pressure stable resonator data when the lasers have the same saturated gain.

comparison of the same saturated gain cases should be noted. First, the ratio of CL I to CL II powers is larger for the same saturated gain case and second, this ratio is pressure dependent for the same saturated gain case, but pressure independent for the same cavity loss case. These differences indicate that when comparing las r performance, it is important to know if the lasers have the same cavity loss or the same saturated gain. These data show that, if the saturated gain is kept constant, for only a 25% performance penalty, the size, weight, and gas flow rates can be reduced by a factor of two.

Comparison of the power spectral distributions of the CL I to those of the CL II[4] for the same saturated gain shows that the spectra are similar, see Figures 14 and 17. The minimum at $P_2(11)$ occurs in the CL II spectra for both low and high pressures, and is more pronounced in the high pressure cases, but the $P_2(11)$ minimum only occurs for high pressure in the CL I spectra. This is probably a result of nonlinear scaling effects.

Comparison of the beam diameters of the two lasers having the same saturated gain shows that the beam diameters of the CL I are smaller than those of the CL II, Table 9. For low pressure, the CL I beam diameters are from 1.30 to 1.97 mm smaller than the CL II beam diameters, independent of flow rate. For high pressure, the CL I beam diameters are from 0.15 to 1.05 mm smaller than those of the CL II, also independent of flow rate. The differences between the CL I and CL II beam diameters when the saturated gains are the same are less than when the resonators have the same cavity losses. The difference in the beam diameters of the CL I and CL II lasers, for the same saturated gain case, is a result of the different mirror separations which occurred when EMM were used on the CL II and VMM on the CL I. Calculation of beam radii from the equations of Reference 10 showed that VMM

2.2.1 COMPARISON OF BLAZE II CALCULATIONS WITH DATA

The CL I Blaze II results are compared to data in Tables 1-4, 7 and 8 as well as graphically in Figures 20, 21 and 22. The Blaze II computer simulations agree very well with the experimental data; in particular the slopes of the Blaze II and data curves in Figures 20-22 are in good agreement. The largest difference between calculation and data occurs in the low pressure beam diameters which Blaze II overpredicts by 0.52 to 2.22 mm, an average of 1.49 mm. Other than this difference, Blaze II tracks the CL I data as well as Blaze II tracks the CL II data[2,3,4,5,8].

Figure 23 shows the CL II Blaze II performance curves. For r_{eff} = 0.46, Table 10, the CL I Blaze II performance is 43% to 46% of the CL II Blaze II performance with an overall average of 44%. This overall average of 44% is nearly the same as the overall average of 45% found when comparing the CL I to the CL II performance data for the same cavity loss, Section 2.1.4.

Comparison of CL I and CL II Blaze II results for the same saturated gain, Table 10, shows that, for low pressure, the CL I Blaze II powers range from 53-56% of the CL II Blaze II powers, an average of 55%. For high pressure, the CL I Blaze II powers range from 55-63% of the CL II Blaze II powers, an average of 58%. These average percentages are not as large as observed in the data comparison, Section 2.1.6, but they do reflect the higher power ratios and the pressure dependence of the power ratios of the same saturated gain case as compared with the same cavity loss case.

The CL I Blaze II results indicate that the set of values for the four input parameters, percent SF_6 dissociation, initial temperature of the flow at the H_2 injectors, and primary and secondary mixing lengths, yields quite acceptable agreement with the measured stable resonator data as a function of flow rate, cavity loss, pressure, and laser size (gain length).

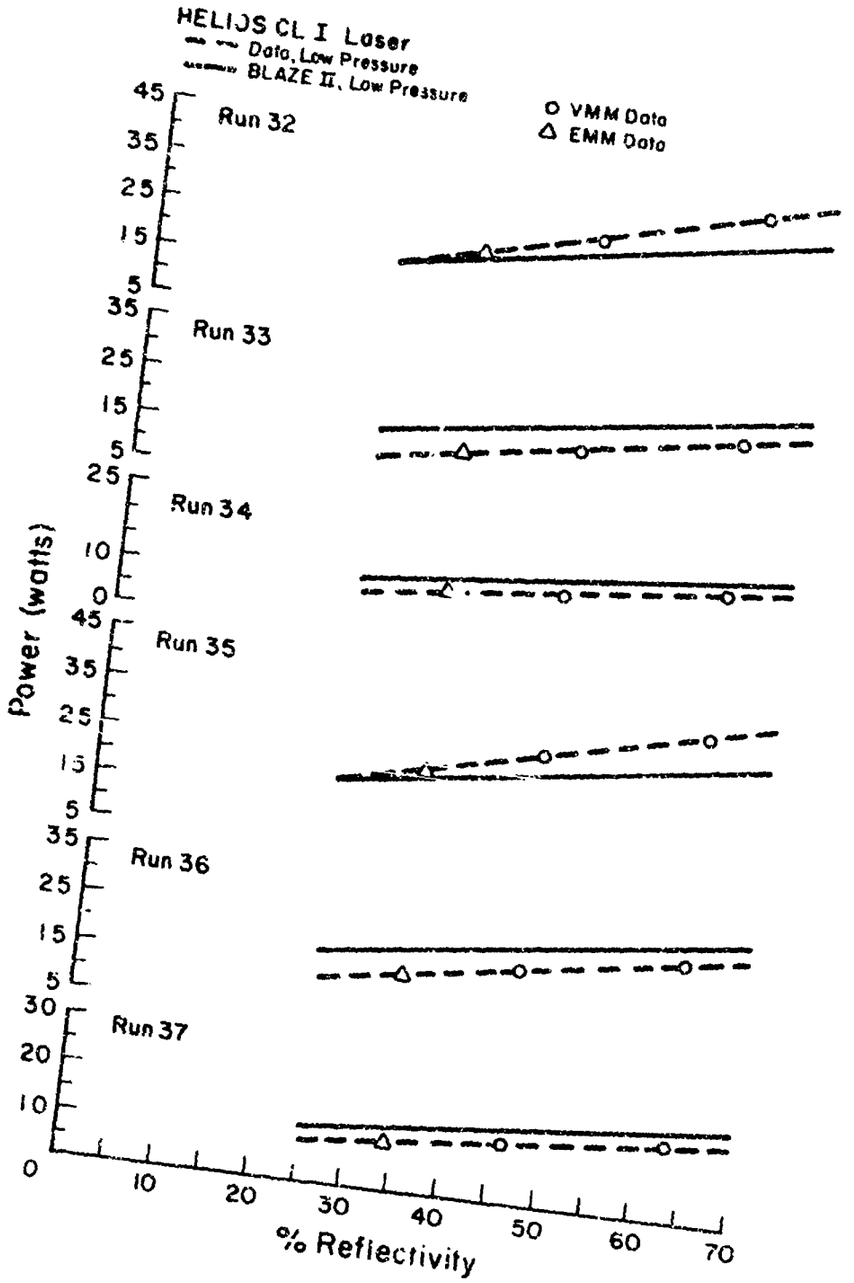

Figure 20. Comparison of low pressure experimental and predicted total power versus % reflectivity for the Helios CL I laser. The EMM data used a 46% reflective outcoupler with the new 4 cm CaF_2 Brewster windows which result in a 34% effective reflectivity.

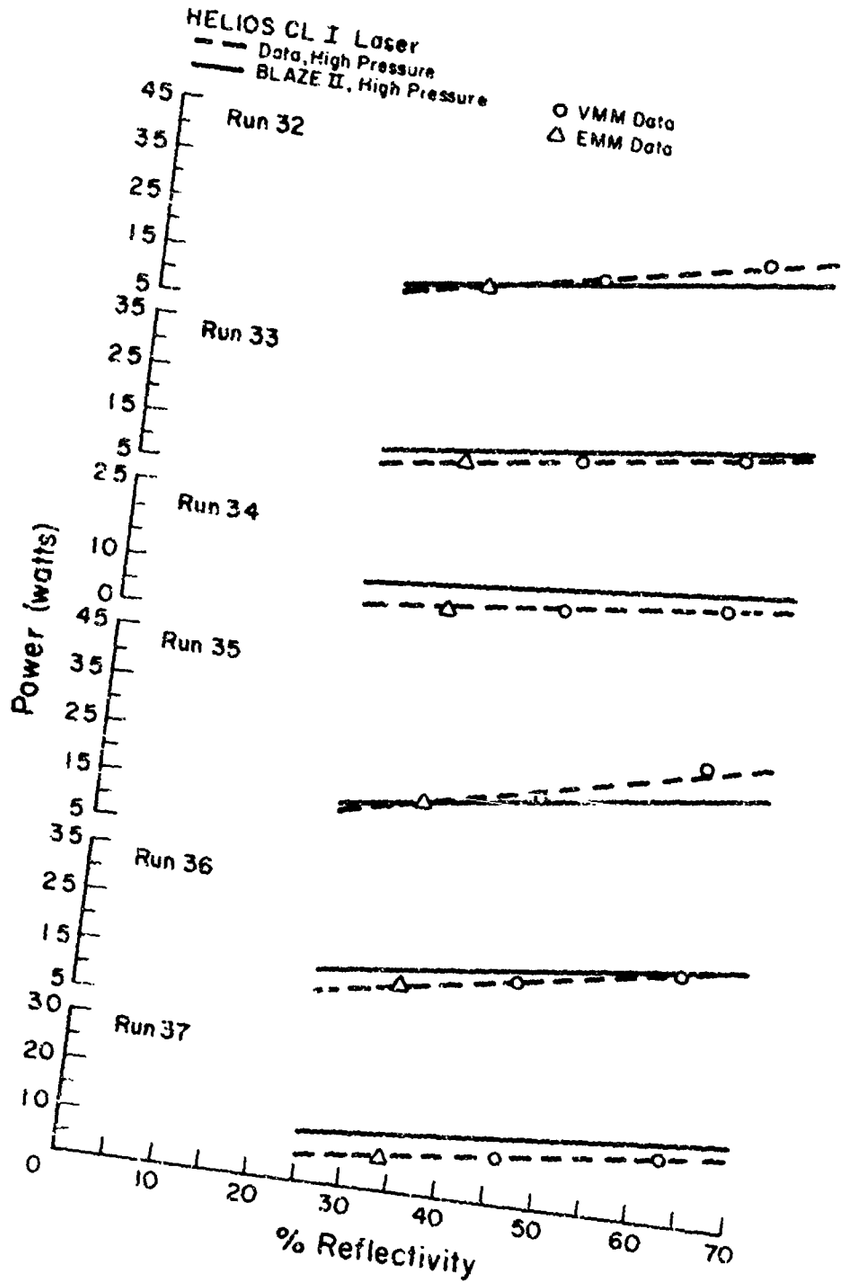

Figure 21. Comparison of high pressure experimental and predicted total power versus % reflectivity for the Helios CL I laser. The EMM data used a 46% reflective outcoupler with the new 4 cm CaF_2 Brewster windows which result in a 34% effective reflectivity.

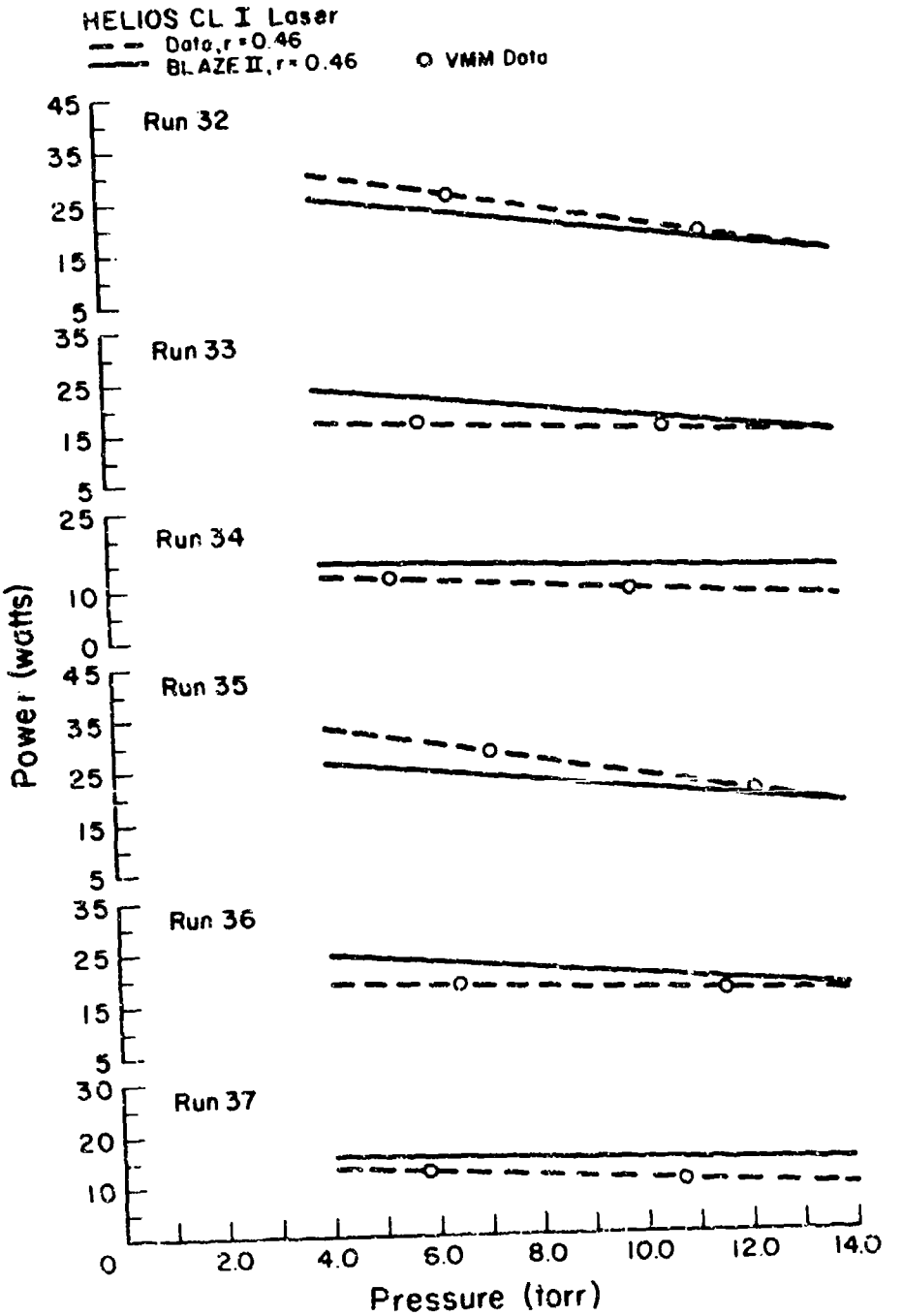

Figure 22. Comparison of experimental and predicted total power versus pressure for the Helios CL I laser with a 46% reflective outcoupler in VMM.

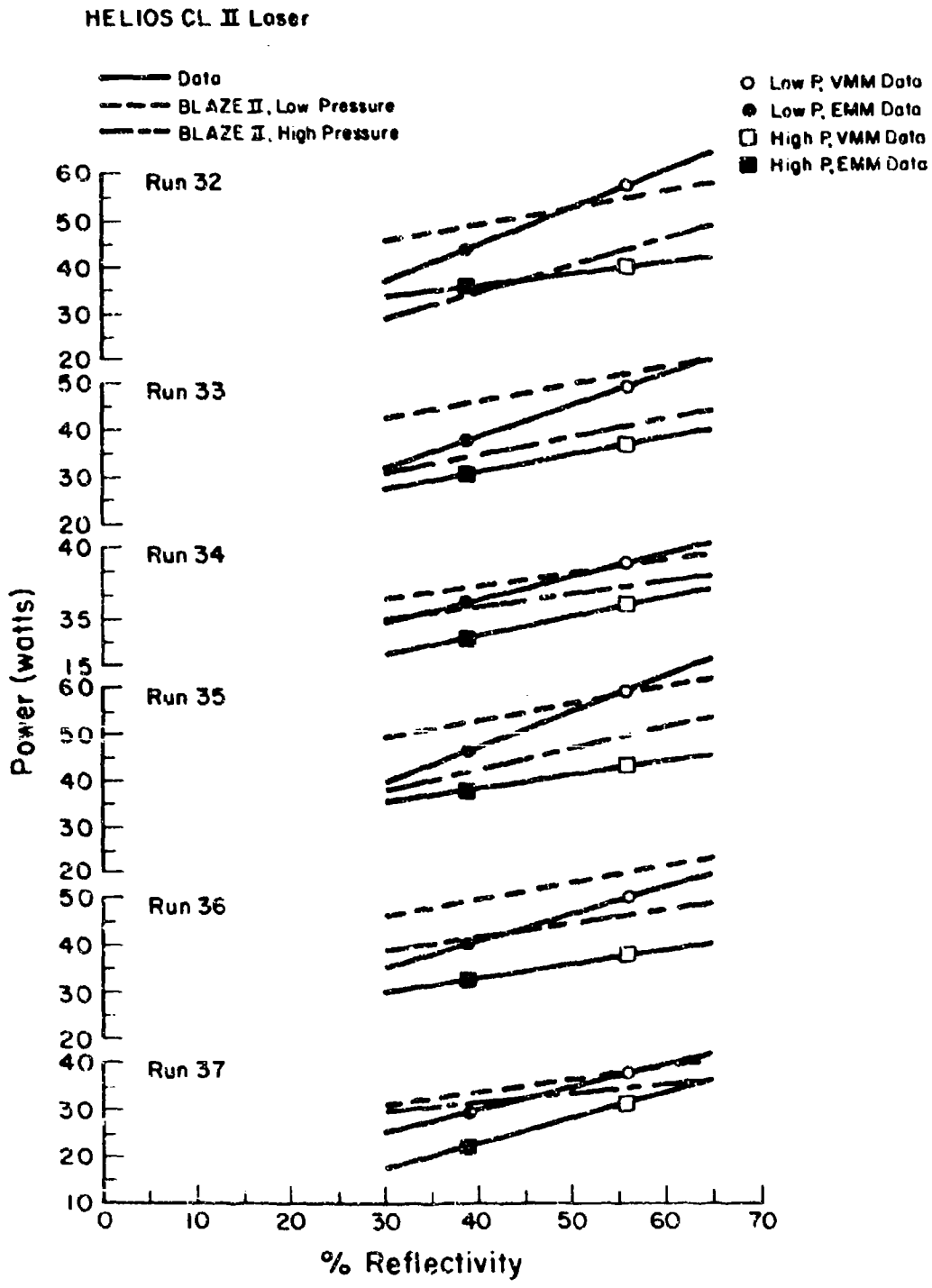

Figure 23. Comparison of the experimental and predicted Helios CL II stable resonator total power versus % reflectivity for low and high pressure.[4]

Same Cavity Loss

	RUN NO.					
	32	33	34	35	36	37
Low Pressure						
CL I, r_{eff} = 0.46	22.1	21.4	14.4	23.7	22.8	15.3
CL II, r_{eff} = 0.46	51.0	47.9	33.3	55.2	51.7	35.1
% (CL I/CL II)	43.3	44.7	43.2	42.9	44.1	43.6
High Pressure						
CL I, r_{eff} = 0.46	16.8	16.9	13.2	19.1	18.9	14.3
CL II, r_{eff} = 0.46	37.6	36.8	29.2	45.0	43.1	32.5
% (CL I/CL II)	44.7	45.9	45.2	42.4	43.9	44.0

Overall average % (CL I/CL II) = 44.0

Same Saturated Gain

Low Pressure						
CL I, r_{eff} = 0.63	26.7	25.5	17.5	28.1	26.8	18.3
CL II, r_{eff} = 0.39	48.5	45.5	31.5	52.6	49.2	33.3
% (CL I/CL II)	55.1	56.0	55.6	53.4	54.5	55.0

Low Pressure Average % (CL I/CL II) = 54.9

High Pressure						
CL I, r_{eff} = 0.63	20.9	20.8	15.9	23.1	22.6	17.0
CL II, r_{eff} = 0.39	33.4	34.0	27.6	41.9	41.2	31.1
% (CL I /CL II)	62.6	61.2	57.6	55.1	54.9	54.7

High Pressure Average % (CL I/CL II) = 57.7

Table 10. Comparison of the Helios CL I and CL II Blaze II total powers when the cavity losses are the same and when the saturated gains are the same for low and high pressure.

2.2.2 COMPARISON OF MNORG3SR CALCULATIONS WITH DATA

The results of Reference 8 showed that the separate baselining of the Fabry-Perot and stable resonator codes accounted for resonator mode structure which is not included in the geometric optics Fabry-Perot and stable resonator models. Because the stable resonator code is very expensive to run, to insure consistency of the stable resonator baselining parameters as a function of flow rates and pressure, the Blaze II code was used to determine these parameters and to compare performance as a function of flow rate and pressure. Since the Fabry-Perot model always gives the largest power, Blaze II was baselined to overpredict the stable resonator data by about 17.5% for all six flow rates. With this set of values for the four input parameters, stable resonator calculations were performed for two flow rates, Runs 34 and 36, at low and high pressure for vacuum and external mirror mount cavities. The agreement between the CL II stable resonator calculations and data was reasonable[8].

As a further check of the validity of the stable resonator model, MNORO3SR calculations were performed for the CL I by reducing the input mass flow rates and gain length by a factor of two. Before the MNORO3SR calculations were performed, Blaze II results were obtained for the CL I for all six flow rates, Table 11. Comparison of CL I and CL II[8] overprediction by Blaze II shows that Blaze II overpredicts the CL I data by an average of 10.2% and overpredicts the CL II data by an average of 8.2%.

With the fluid flow profiles generated by the Blaze II results, two stable resonator calculations were made for the CL I, Runs 34 and 36, low pressure, Table 12. As in the case of the CL II[8], the results give acceptable agreement with the measured total power, power split, and beam diameters. The power spectral distributions, Figures 24 and 25, show that the MNORO3SR

r_{eff} = 0.63, Low P

RUN NO. 32	33	34	35	36	37	
$\dot{m}_{H_2}$ (gm/sec)	0.0228	0.0228	0.0228	0.0305	0.0305	0.0305
$\dot{m}_{SF_6}$ (gm/sec)	0.715	0.535	0.355	0.715	0.535	0.355
Blaze II (Input Data)						
% SF_6 Dissoc.	4.0	4.0	4.0	4.0	4.0	4.0
Initial T (°K)	450	450	450	450	450	450
H_2 Mixing Length	3.5	3.5	2.5	3.5	3.5	2.5
P(Meas.) (Torr)	6.7	6.0	5.4	7.2	6.5	5.8
P_T (Watts)						
Data 33.2	21.6	15.3	35.7	23.0	15.5	
Blaze II	30.0	25.5	18.7	32.1	26.8	19.3
% Over data	-9.6	+18.1	+22.2	-10.1	+16.5	+24.5
P_{10}/P_T						
Data 0.706	0.434	0.347	0.589	0.423	0.568	
Blaze II	0.504	0.492	0.483	0.503	0.493	0.484
Beam Dia. (mm)						
Data 3.60	3.03	3.45	2.70	2.46	3.00	
Blaze II	5.14	5.24	4.30	4.09	4.18	3.46

Table 11. Summary of the low pressure stable resonator data and Blaze II results for the Helios CL I with a 63% reflective outcoupler in VMM. The Blaze II parameters were those used for MNORO3SR CL II calculations[8].

Case	Total Power (Watts)	P_{10}/P_T	Beam Dia. (mm)
RUN 34			
Data, VMM	15.3	0.447	3.45
MNORO3SR (OA = 0.250 cm)	16.8	0.488	4.92
RUN 36			
Data, VMM	23.0	0.423	2.46
MNORO3SR (OA = 0.225 cm)	23.9	0.501	4.43

Table 12. Summary of the low pressure stable resonator data and MNORO3SR results for the Helios CL I with a 63% reflective outcoupler in VMM.

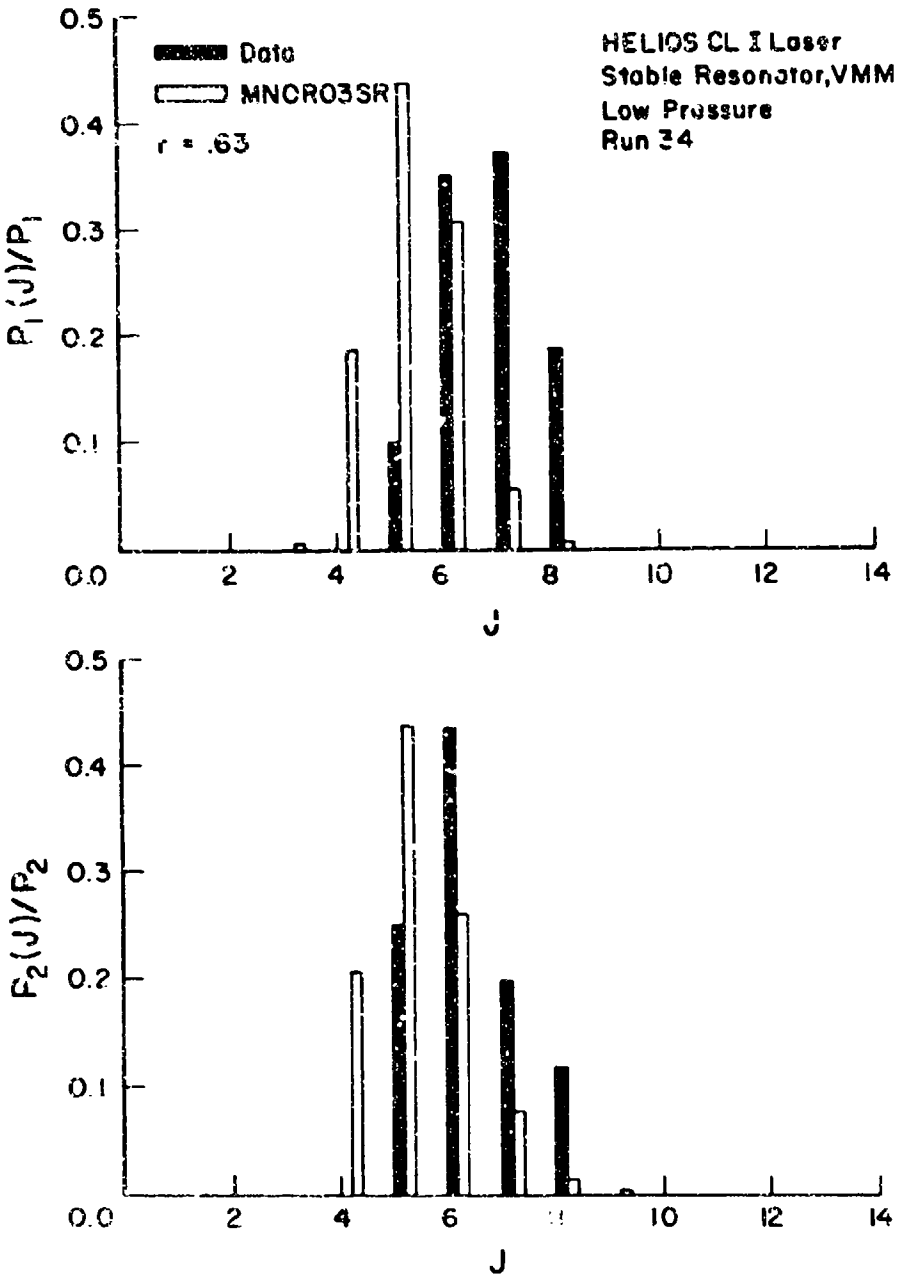

Figure 24. Comparison of the Helios CL I low pressure experimental and MNORO3SR power spectral distributions for RUN 34 using VMM, r = 0.63, optical axis = 0.250 cm.

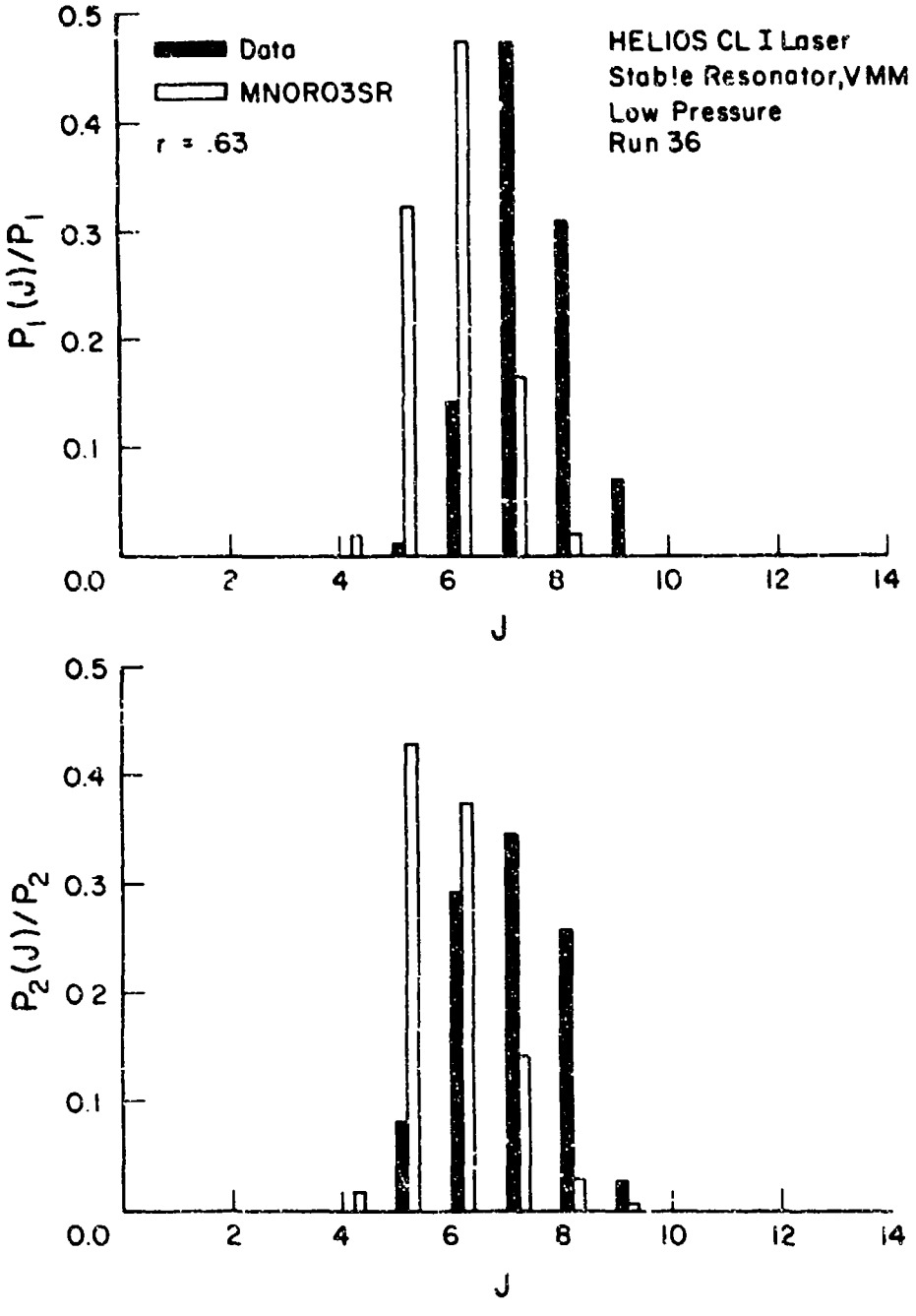

Figure 25. Comparison of the Helios CL 1 low pressure experimental and MNORO3SR power spectral distributions for RUN 36 using VMM, r = 0.63, optical axis = 0.225 cm.

spectral peaks are shifted one J lower than the data. This shift was also observed when comparing CL II MNORO3SR spectra to measured CL II spectra[8].

In summary, the Blaze II and MNORO3SR CL I calculations track the CL I data as well as these models tracked CL II data. This shows that these computer models are valid as a function of mass flow rates, cavity losses, pressure and size of the laser.

2.3 SUMMARY OF CL I STABLE RESONATOR RESULTS

Several scale effects were observed when comparing CL I stable resonator data with CL II stable resonator data. When the resonators have the same cavity losses, the CL I power was an average of 45% of the CL II power. The slopes of the power versus reflectivity curves are steeper for the CL II than for the CL I, except for the high pressure, highest SF_6 flow rates. The spectral peaks of the CL I laser are shifted one J lower than the spectral peaks of the CL II laser. The CL I spectra show the appearance of lower J lines and the loss of higher J lines when compared to CL II spectra having the same cavity loss. Fewer lines are observed in the power spectral distributions of the CL I laser. The beam diameters of the CL I laser are smaller than those of the CL II laser. These scale effects are all pressure independent and are a consequence of the CL I laser having twice the saturated gain of the CL II laser.

Different scale effects are observed when the CL I and CL II resonators have the same saturated gain. The CL I power varied from 52-80% of the CL II power; for the high SF_6 flow rates, the CL I power was 70-80% of the CL II power. These data indicate that if the saturated gain is kept constant as the size of the laser is reduced, it may be possible to reduce the size, weight and gas flow rates by a factor of two with only a 25% performance penalty. The power spectral distributions of the two resonators having the same

saturated gain are similar, including the minimum at $P_2(11)$ for high pressure. The beam diameters of the CL I laser are smaller than those of the CL II laser. The difference between the beam diameters of the CL I and CL II lasers when the saturated gains are the same is less than when the two resonators have the same cavity loss. For the same saturated gain case, the difference between CL I and CL II beam diameters is a result of the different mirror separations which occurred when EMM were used on the CL II and VMM on the CL I.

Both the Blaze II and MNORO3SR computer simulations gave good agreement with the measured CL I power, power split, and beam diameters. MNORO3SR computations produced power spectral distributions which were in reasonable agreement with the CL I data. These calculations show that the Blaze II and MNORO3SR computer models of the Helios laser are valid as a function of mass flow rates, cavity losses, pressure and size of the laser.

III. CL I CONFOCAL UNSTABLE RESONATOR PERFORMANCE

To study the effects of temporal variations in the CL I oscillator on the CL II amplifier performance, the time-dependent oscillations of the CL I oscillator must be known. Thus the CL I laser was characterized with an unstable resonator. To compare with the CL II unstable resonator data[3], the same 50% geometric outcoupled, confocal unstable resonator with a variable slit scraper mirror was used on the CL I. The experimental results are presented in the subsequent sections.

3.1 ALIGNMENT PROCEDURE

Figure 25 shows the layout of the 50% geometric outcoupled, confocal unstable resonator used on the Helios CL I laser. The resonator consists of a convex and a concave mirror separated by one meter, with a flat slit scraper mirror placed at an angle of 45° to the optical axis near the convex mirror. The radius of curvature of the mirrors is -2 meters for the convex mirror and 4 meters for the concave mirror which result in a resonator magnification of 2. The slit scraper mirror consists of two flat mirrors which slide apart to form a slit whose width can be varied from 0.0 to 10.0 millimeters. Since the resonator is a confocal unstable resonator with a magnification of 2, the effective diameter of the convex mirror is equal to the scraper mirror slit width and the effective diameter of the concave mirror is equal to twice the scraper mirror slit width. The Fresnel number for the resonator is given by

$$N_F = \frac{D^2}{4\lambda L} \qquad (3.1\text{-}1)$$

where D is the diameter of the large mirror, λ is the wavelength and L is the mirror spacing. For this resonator, the Fresnel number is determined by the effective diameter of the concave mirror and is therefore controlled by the

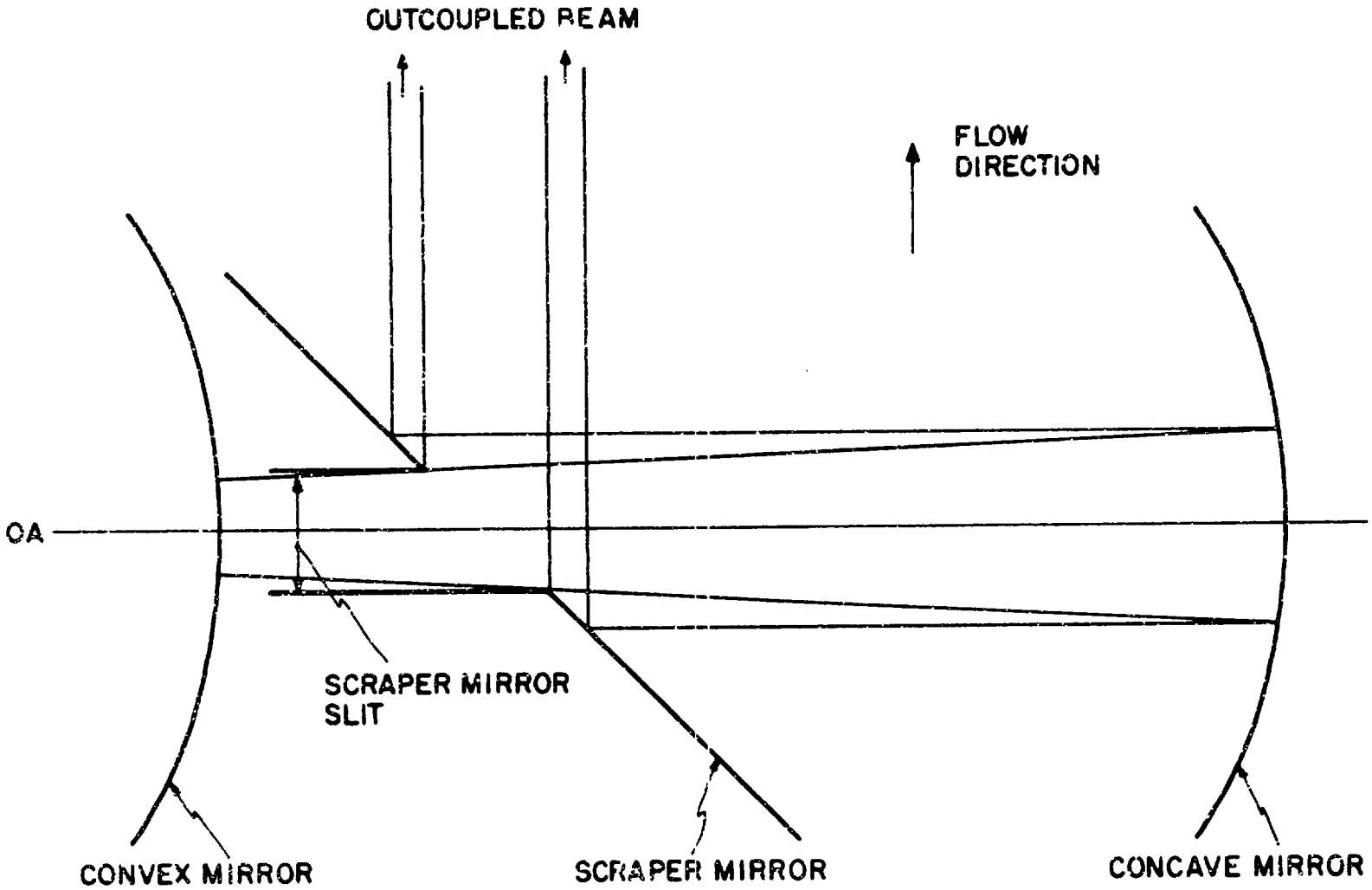

Figure 26. Layout of the unstable resonator used in the measurement of the time-dependent oscillations on lines whose saturated gain does not fill the resonator.

slit width of the craper mirror. The Fresnel number for the resonator used on the Helios CL I laser ranged from 0.0 to 8.9.

The alignment procedure for the CL I is the same as that described in Reference 3; however, for completeness the alignment procedure will be repeated. Figure 27 shows the optical path of the alignment HeNe laser through the unstable resonator. The resonator's mirrors are mounted on a set of translation stages, which allow accurate positioning of the optical axis of the resonator with respect to the H_2 injectors. The unstable resonator alignment procedure consists of five steps.

The first step is to align the HeNe laser beam with the H_2 injectors of the laser. Note that for this step, the Brewster windows and the resonator mirrors were not in their mounts. The HeNe laser is set at a height equal to the height of the center of the laser cavity plus the necessary additional height to compensate for the refraction offset due to the right Brewster window when it is in place. An iris mounted on a magnetic base, which was set to the height of the HeNe laser beam, was used to check that the HeNe beam was at the proper height throughout the alignment procedure. The HeNe beam was split into two components as shown in Figure 27. Mirror 1 was then adjusted until beam 1 was aligned with the H_2 injectors in the laser cavity. The right Brewster window was then attached to the laser. Fine adjustments were made to mirror 1 until the beam exited the left side of the laser cavity centered both vertically and parallel to the H_2 injectors. The left Brewster window was then attached to the laser and the height of the HeNe was checked with the iris at the far left of the laser. If necessary, mirror 1 was adjusted again to correct any error in the alignment of the HeNe beam with respect to the laser cavity.

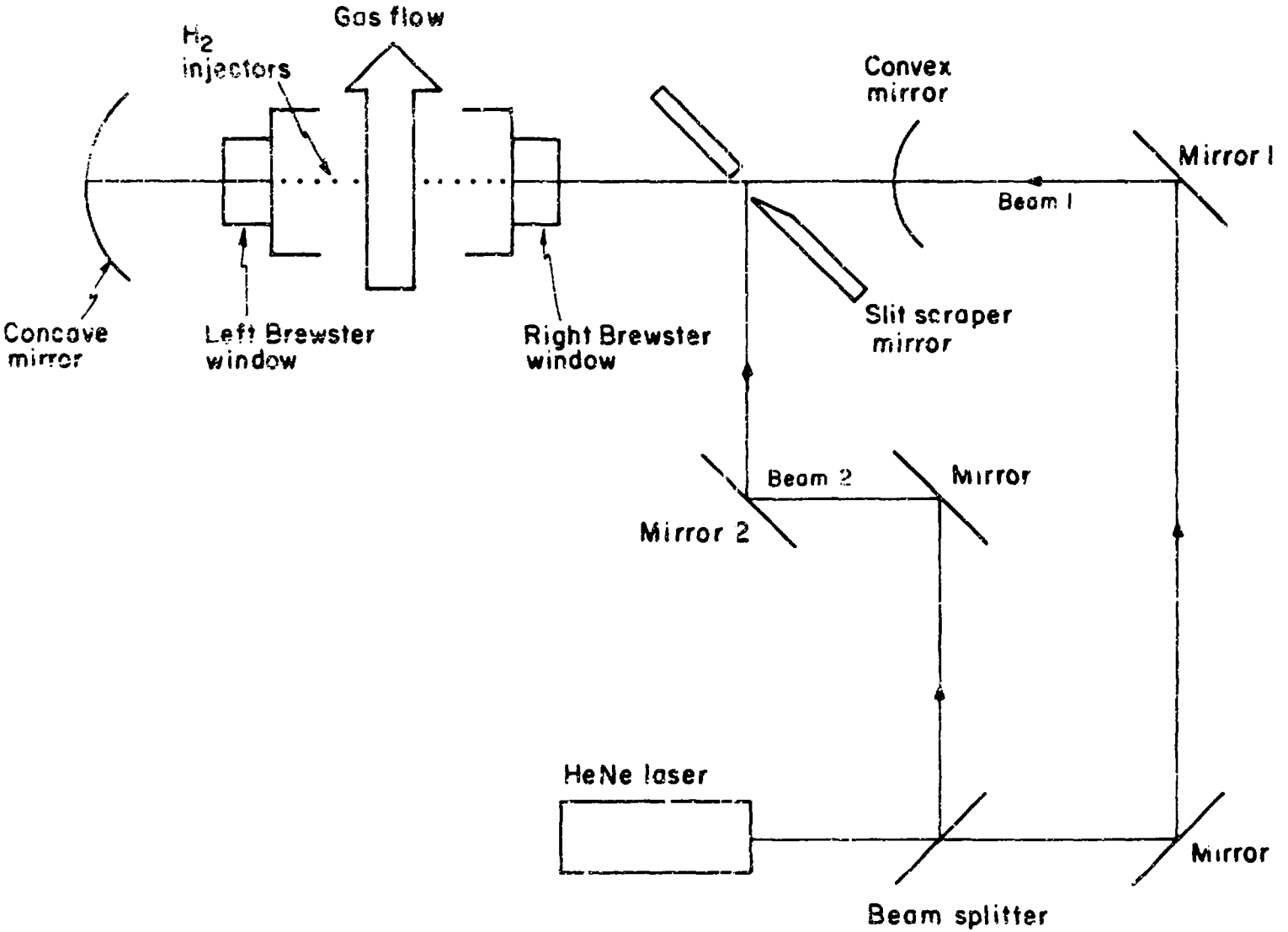

Figure 27. Optical path of the HeNe alignment laser through the confocal, unstable resonator.

The second step in the alignment procedure was to center the mirror holders on the HeNe beam aligned in the first step. The translation stages are located on the optical table so that their range of travel permits movement of the optical axis both upstream and downstream of the H_2 injectors. The alignment of the mirror holders on the translation stages was achieved by using two plexiglas disks which fit into the mirror mounts. Each disk had a small hole the diameter of the HeNe beam drilled in its center. The mounts were then positioned on the translation stages so that the alignment beam passed through each hole.

The third step was the alignment of the concave mirror. The concave mirror was placed in its mount and then tuned until beam 1 reflects back upon itself.

The fourth step was the alignment of the slit scraper mirror. The variable slit scraper mirrors were placed in their mounts and the slit was fully opened. The position of each half of the variable slit scraper mirror is controlled by a micrometer. Each side, in turn, was moved in until it blocked out beam 1 and the micrometer reading was recorded. The micrometers are then both set shorter than the previous reading by half the diameter of the HeNe beam. The mirror halves would just touch at this setting. Then each mirror is moved out by one millimeter on the micrometer. The HeNe image reflected back by the concave mirror will then appear symmetric about the scraper mirror slit. Mirror 2 was then adjusted until beam 2 was centered on the slit and the image of beam 1 from the scraper mirror was symmetric about beam 2 on mirror 2 and on the face of the HeNe laser. A check of the alignment was to block beam 1 and the image of beam 2 reflected off the scraper mirrors would be symmetric and centered about the H_2 injectors on both sides of the laser cavity.

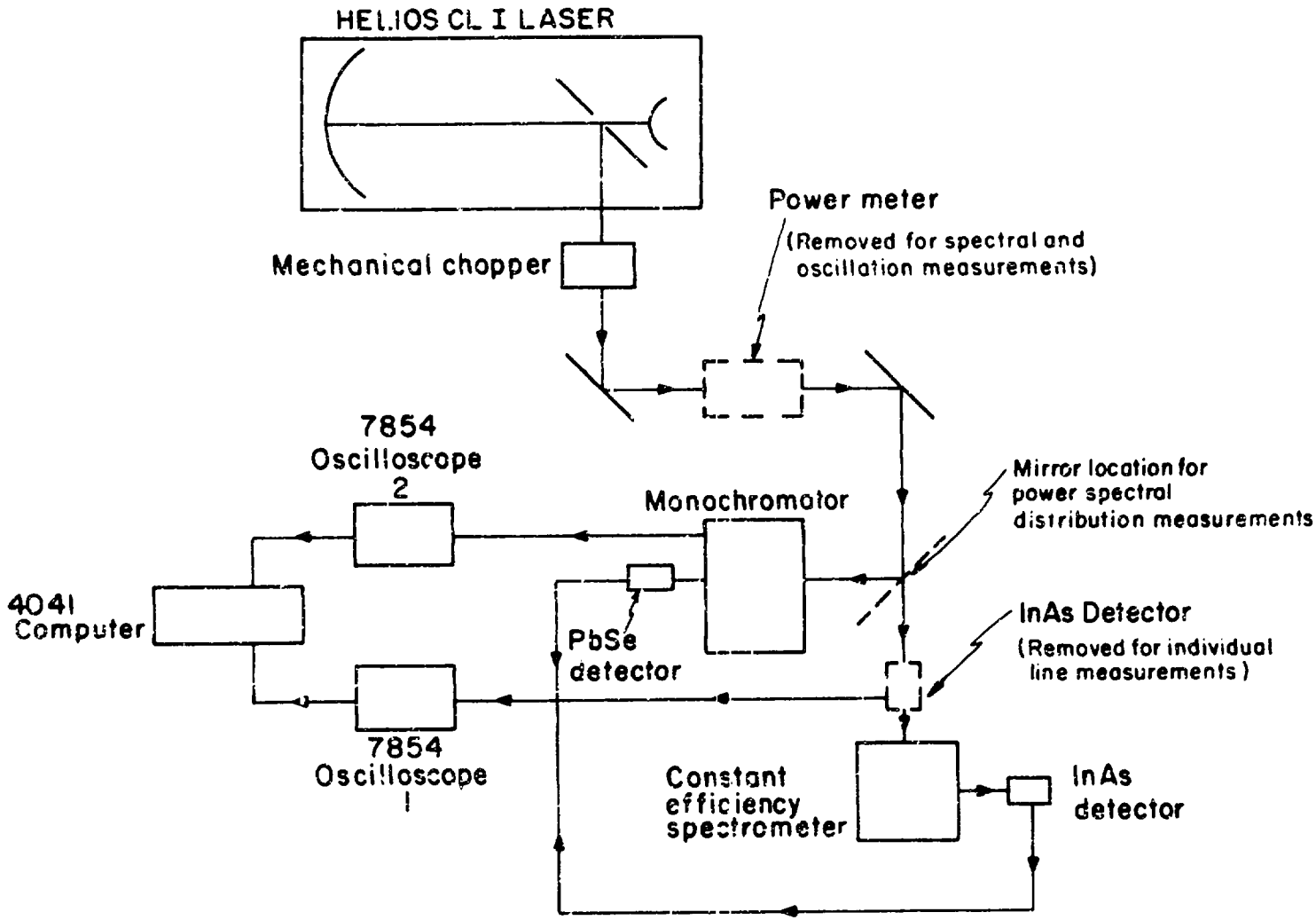

Figure 28. Schematic of the experiment to measure the time-dependent oscillations on lines whose saturated gain does not fill the unstable resonator.

and the H_2 injectors was always equal to the scraper mirror slit width. A summary of the total power unstable resonator data for Run 34 is presented in Table 13. Both 47 ns and 7 ns oscillations were observed in the CL I unstable resonator. The 47 ns oscillation did not occur for Fresnel numbers below 3.2. As observed in Reference 3, the 7 ns oscillation was superimposed on the 47 ns oscillation. Since the round trip transit time of a photon is 6.67 ns (the mirror spacing is 1 meter), the 7 ns oscillation most likely corresponds to a mode beat of the laser. Figure 29 shows the digitized 7 ns oscillation superimposed on the 47 ns oscillation as well as the corresponding square wave which results from the beam chopper. The corresponding spectrum analyzer trace is shown in Figure 30. From the spectrum analyzer trace, it is seen that the long period oscillation is 21.1 MHz (47 ns) and the short period oscillation is 143 MHz (7 ns).

Table 14 gives the oscillation data for individual lines as a function of Fresnel number. This data shows that the 47 ns oscillation on lines whose saturated gain does not fill the resonator do not occur for Fresnel numbers below 3.2. The appearance of the 47 ns oscillation on only one line, $P_1(7)$, should be noted. This occurs because the power of most of the individual lines was too small to drive the fast InAs detector.

3.4 RUN 36, LOW PRESSURE DATA

Total power, oscillation frequency and amplitude measurements for Run 36, the middle SF_6 and high H_2 flow rates, were taken at a pressure of 6.50 torr. Since a symmetric resonator was used, the distance between the optical axis and the H_2 injectors was always equal to the scraper mirror slit width. A summary of the total power unstable resonator data for Run 36 is presented in Table 15. Again the total powers are small and both the 47 ns and 7 ns oscillations appear. The 47 ns oscillation on lines whose saturated gain does

CL I Run 34, 5.40 Torr, 50% Geometric Outcoupled,
Symmetric, Confocal, Unstable Resonator

Scrapper Mirror Slit (mm)	N_F	P_T (Watts)	OSC Period (ns)	Amplitude Modulation (% P_T)
1.0	0.357	0.39	--	--
2.0	1.428	1.97	7	5.3
3.0	3.214	1.03	7	4.7
4.0	5.714	0.10	47/7	50.1
5.0	8.929	0.01	--	--

Table 13. Frequency and amplitude of the time-dependent oscillation of total power as a function of Fresnel number for the flow rates of RUN 34 at 5.4 torr.

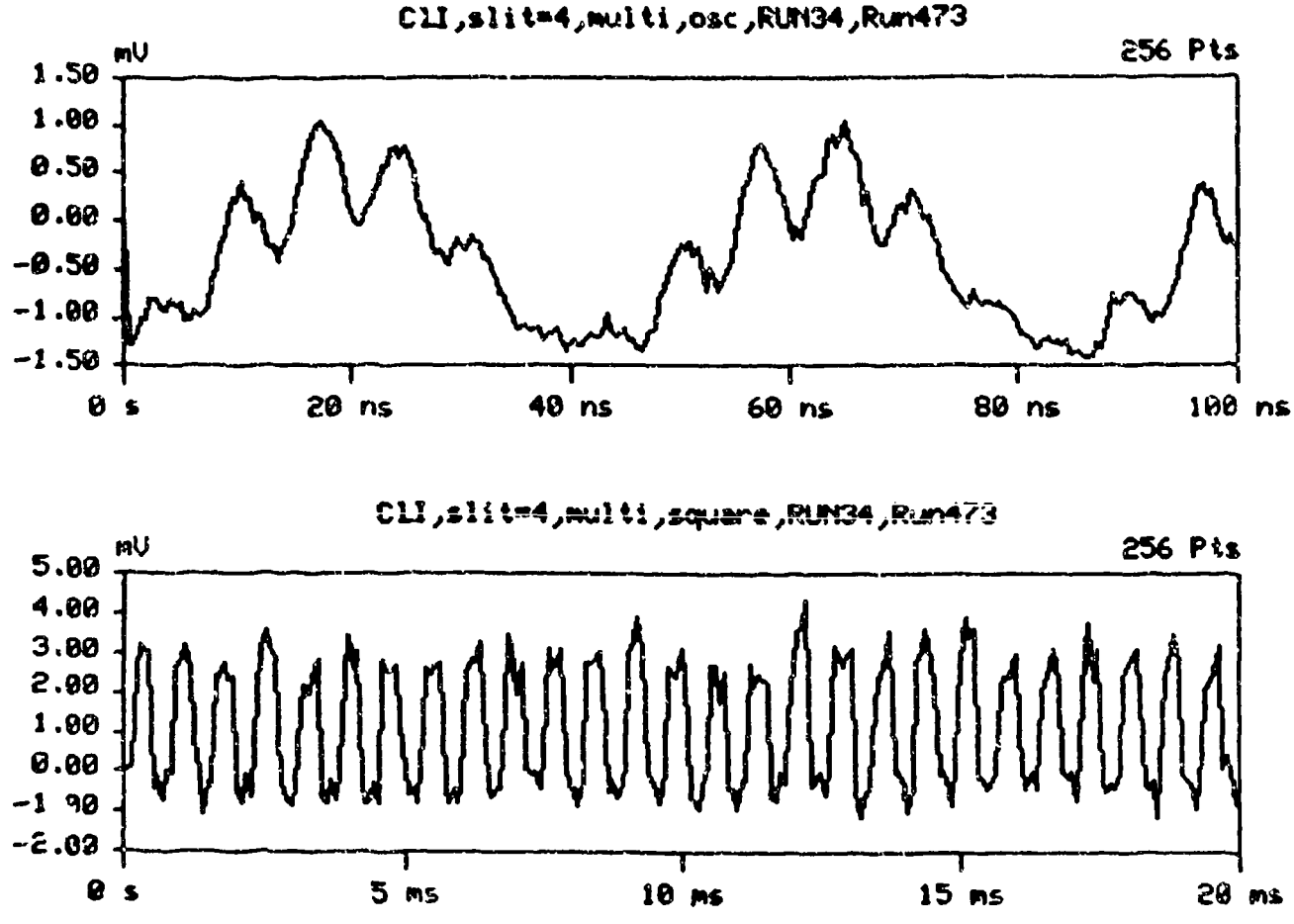

Figure 29. Typical oscilloscope traces of the time-dependent oscillations of the total power when the saturated gains of some of the lasing lines do not fill the unstable resonator. These data are for a scraper mirror slit width of 4 mm for the RUN 34 flow rates at 5.4 torr. The 47 ns oscillation with the superimposed 7 ns oscillation is clearly evident in the upper trace. The lower trace shows the square wave which results from the beam chopper. From the vertical scale of these traces, the percent amplitude modulation induced by the 47 ns oscillation was calculated.

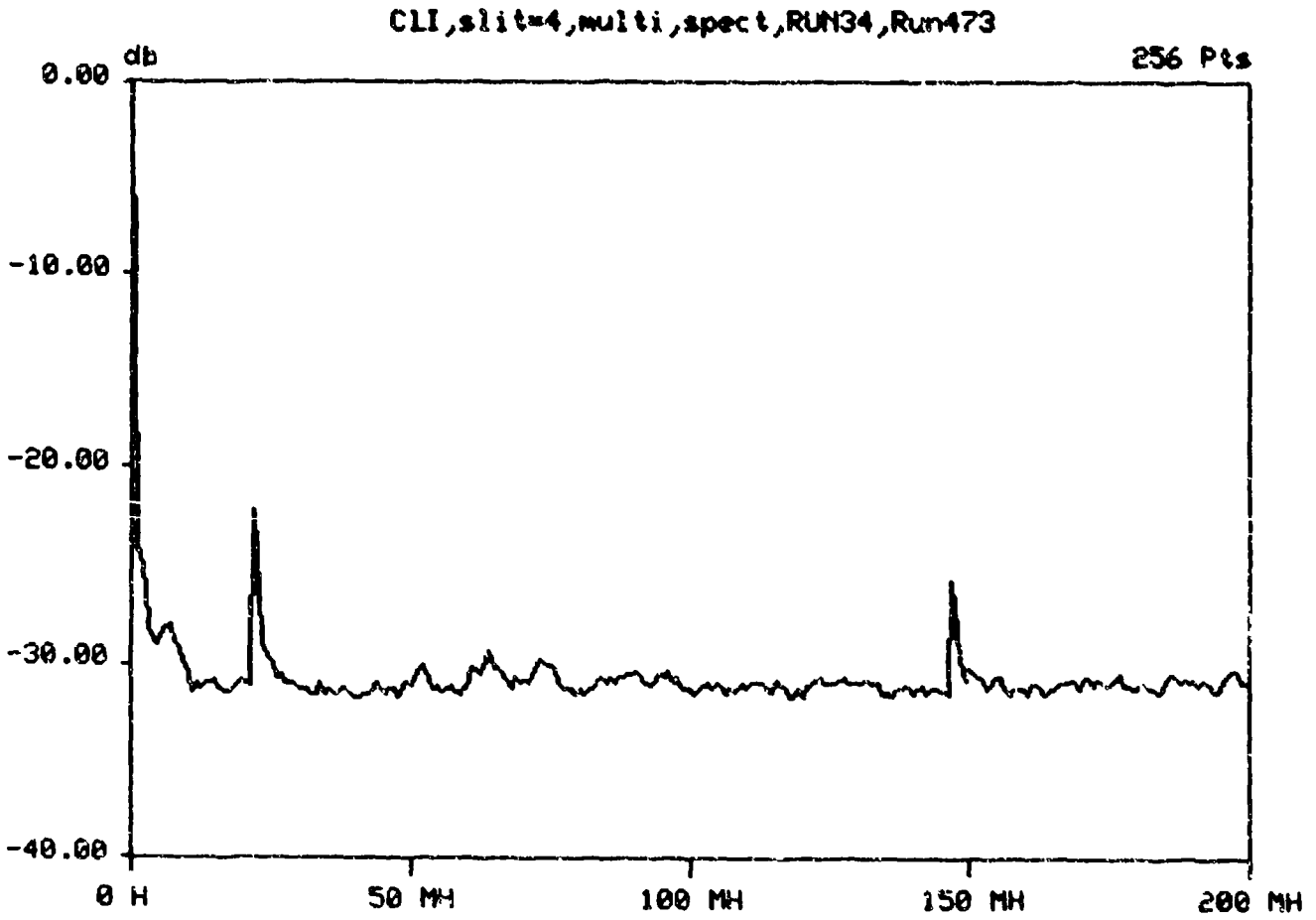

Figure 30. The spectrum analyzer trace for the total power oscillations shown in Figure 29 clearly shows the 47 ns (21.1 MHz) and 7 ns (143 MHz) oscillations.

CL I, Run 34, 5.40 Torr, 50% Geometric Outcoupled,
Symmetric, Confocal, Unstable Resonator

Scraper Mirror Slit (mm)	N_F	Lasing Line	$P_1(6)$	$P_1(7)$	$P_1(8)$	$P_2(5)$	$P_2(6)$	$P_2(7)$	$P_2(8)$	P_T (Watts)
2.0	1.428	OSC Period (ns)	7	7		--	7	7		1.97
		Amplitude Modulation % P_v(J)	24.1	17.6			25.0	28.5		
3.0	3.214	OSC Period (ns)	--	--	--		7	7		1.03
		Amplitude Modulation % P_v(J)					22.5	13.9		
4.0	5.714	OSC Period (ns)		47/7				--		0.10
		OSC Freq. (MHz)		21.1						
		Amplitude Modulation % P_v(J)		34.6						

-- Means that the line lased but was too weak to operate the fast detector.

Table 14. Frequency and amplitude of the time-dependent oscillations on individual lines for the flow rates of RUN 34 at 5.4 torr as a function of Fresnel number. Individual line data were not taken for the 5 mm slit because the individual lines in this case were too weak to operate the fast detector.

CL I, Run 36, 6.50 Torr, 50% Geometric Outcoupled,
Symmetric, Confocal, Unstable Resonator

Scraper Mirror Slit (mm)	N_F	P_T (Watts)	OSC Period (ns)	Amplitude Modulation (% P_T)
1.0	0.357	1.08	--	--
2.0	1.428	2.59	7	3.7
3.0	3.214	1.22	7	2.9
4.0	5.714	0.11	47/7	15.5
5.0	8.929	0.01	40	80.8

Table 15. Frequency and amplitude of the time-dependent oscillation of total power as a function of Fresnel number for the flow rates of RUN 36 at 6.5 torr.

not fill the resonator do not occur for Fresnel numbers less than 3.2.

Table 16 gives the oscillation data for individual lines as a function of Fresnel number. The 47 ns oscillation was observed on only one line, $P_1(8)$. Other lines may have had oscillations, but their power was too small to operate the fast detector. Figure 31 shows the digitized 47 ns and 7 ns oscillations of the $P_1(8)$ line. The corresponding square wave is shown in Figure 31 and the spectrum analyzer trace is shown in Figure 32. The spectrum analyzer trace shows that there is a weaker 88 MHz signal as well as the 21.1 MHz (47 ns) and the 143 MHz (7 ns) oscillations. This 88 MHz signal is broad and indistinct and is believed to be random noise in the signal.

3.5 COMPARISON OF CL I AND CL II UNSTABLE RESONATOR PERFORMANCE

Comparison of the CL I and CL II[3] oscillation data shows that no 47 ns oscillations were observed with the 3 mm slit size for the CL I, whereas the CL II showed oscillations of about 40 ns. For the 4 mm slit size, the CL I showed only one individual line with the 47 ns oscillation for each flow rate while the CL II showed six lines with oscillations of about 40 ns for RUN 34 and five for RUN 36. The small number of individual lines which show oscillations can be explained by the fact that the saturated gain of the CL I was twice as large as that of the CL II. Consequently, most of the individual lines did not lase or were too weak to drive the InAs fast detector and thus fewer lines were observed to have oscillations.

The amplitude modulations, $\%P_T$ and $\%P_V(J)$, of the CL I and CL II unstable resonators are similar. For both lasers, the amplitude modulation increased as the fraction of the resonator filled by the saturated gain of a lasing line decreased.

Comparison of the CL I unstable resonator powers, Tables 13-16, with the CL II performance[3] shows a large difference in power. For example, at the

CL I, Run 36, 6.50 Torr, 50% Geometric Outcoupled,
Symmetric, Confocal, Unstable Resonator

Scraper Mirror Slit (mm)	N_F	Lasing Line	$P_1(6)$	$P_1(7)$	$P_1(8)$	$P_2(5)$	$P_2(6)$	$P_2(7)$	$P_2(8)$	P_T (Watts)
2.0	1.428	OSC Period (ns)	--	7	7		--	--	--	2.59
		Amplitude Modulation % $P_v(J)$		30.9	20.1					
3.0	3.214	OSC Period (ns)	--	--	7			--	--	1.22
		Amplitude Modulation % $P_v(J)$			20.9					
4.0	5.714	OSC Period (ns)		--	47/7	--				0.11
		OSC Freq. (MHz)			21.1					
		Amplitude Modulation % $P_v(J)$			57.0					

-- Means that the line lased but was too weak to operate the fast detector.

Table 16. Frequency and amplitude of the time-dependent oscillations on individual lines for the flow rates of RUN 36 at 6.5 torr as a function of Fresnel number. Individual line data were not taken for the 5 mm slit because the individual lines in this case were too weak to operate the fast detector.

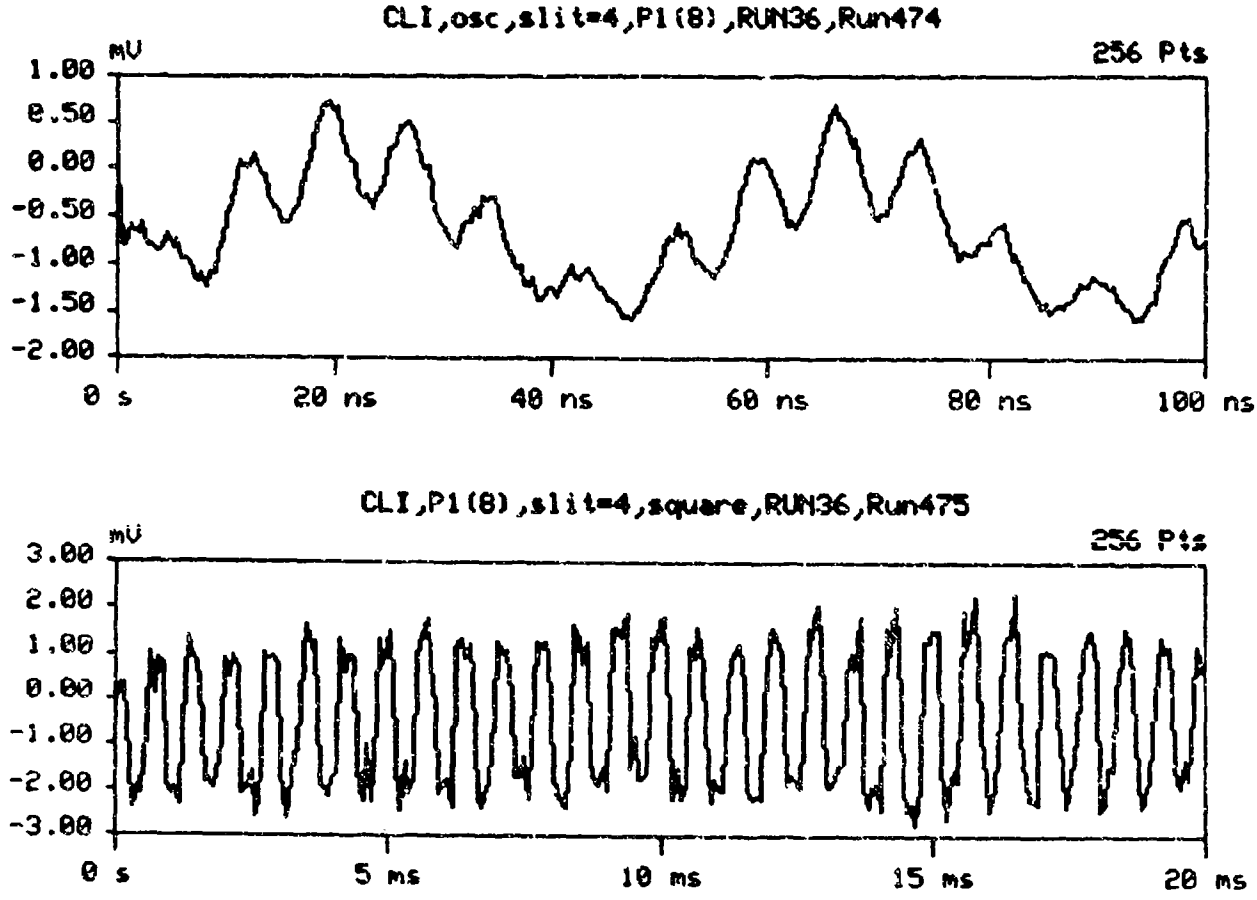

Figure 31. Typical oscilloscope traces of the time-dependent oscillation on a line whose saturated gain does not fill the unstable resonator. These data are for the $P_1(8)$ line for a scraper mirror slit width of 4 mm for the RUN 36 flow rates at 6.5 torr. The 47 ns oscillation with the superimposed 7 ns oscillation is clearly evident in the upper trace. The lower trace shows the square wave which results from the beam chopper. From the vertical scale of these traces, the percent amplitude modulation induced by the 47 ns oscillation was calculated.

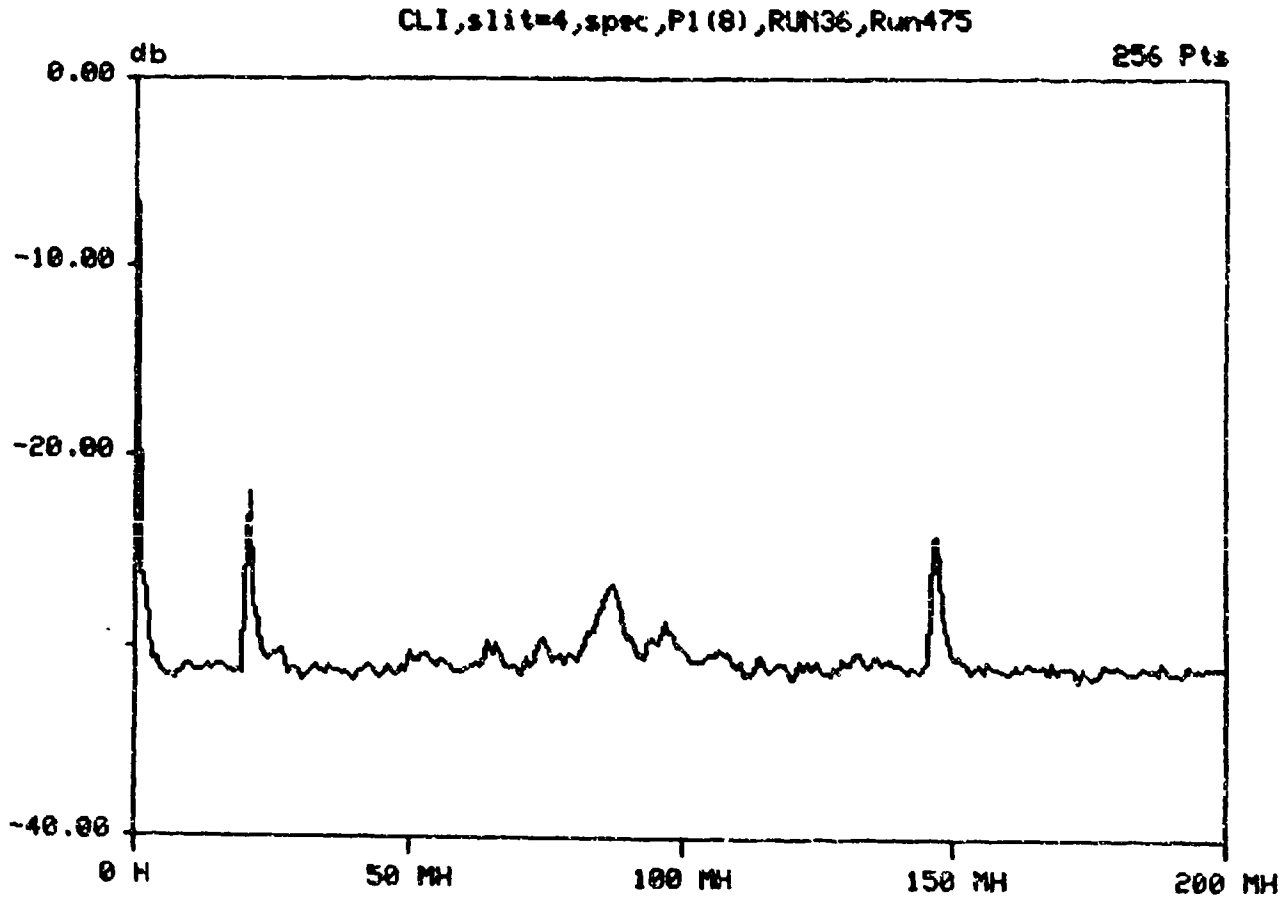

Figure 32. The spectrum analyzer trace for the same line as shown in Figure 31 clearly shows the 47 ns (21.1 MHz) and the 7 ns (143 MHz) oscillations. The trace also suggests the presence of a weak, broad signal at about 86 MHz, which is believed to be random signal noise.

2 mm slit width, the ratio of CL I power to CL II power is 17% for Run 34 and 15% for Run 36. These percentages are considerably lower than the overall average of 45% observed for stable resonator data. A possible explanation for the low CL I unstable resonator output powers is given in the following analysis.

From Reference 10, the saturated gain of a stable or unstable resonator is given by

$$\alpha_{sat} = \frac{1}{2L_e} \ln \left(\frac{M^2}{r_0 r_L} \right) \qquad (3.5\text{-}1)$$

where M is the cavity magnification (M = 1.0 for a stable resonator). Solving for $e^{2L_e\alpha_{sat}}$ gives

$$e^{2L_e\alpha_{sat}} = \frac{M^2}{r_0 r_L} \qquad (3.5\text{-}2)$$

The unstable resonator was 50% geometric outcoupled and thus it is reasonable to make a comparison between the saturated gain of this unstable resonator and the saturated gain of a stable resonator with an effective reflectivity of 50%. The magnification of the unstable resonator was 2.0 and the mirror reflectivities were effectively 1.0. For the stable resonator, the magnification is 1.0 and $r_L = 1.0$ and $r_0 = 0.50$. With these values, Eq. (3.5-2) gives

$$\left(e^{2L_e\alpha_{sat}}\right)_{UR} = 2^2 \qquad (3.5\text{-}3)$$

$$\left(e^{2L_e\alpha_{sat}}\right)_{SR} = 2 \qquad (3.5\text{-}4)$$

Comparison of these results shows that

$$\left(e^{2L_e\alpha_{sat}}\right)_{UR} = \left(e^{2L_e\alpha_{sat}}\right)^2_{SR} \tag{3.5-5}$$

where UR stands for unstable resonator and SR stands for stable resonator. Equation (3.5-5) suggests that the following relationship may exist between the stable and unstable resonators

$$P_{UR} = b_1(P_{SR})^2 \tag{3.5-6}$$

where P stands for power and b_1 is a constant which depends upon flow rates.

If Eq. (3.5-6) was true, then the CL I unstable resonator peak powers could be predicted by

$$\frac{(P_{UR})_{CL\ I}}{(P_{UR})_{CL\ II}} = \frac{(P_{SR})^2_{CL\ I}}{(P_{SR})^2_{CL\ II}} \tag{3.5-7}$$

Thus the expected CL I unstable resonator peak powers for RUN 34 would be

$$(P_{UR})_{CL\ I} = (11.7\ \text{Watts})\left(\frac{12.\ \text{Watts}}{33.5\ \text{Watts}}\right)^2 = 1.63\ \text{Watts} \tag{3.5-8}$$

and for RUN 36

$$(P_{UR})_{CL\ I} = (17.2\ \text{Watts})\left(\frac{19.6\ \text{Watts}}{46.5\ \text{Watts}}\right)^2 = 3.06\ \text{Watts} \tag{3.5-9}$$

The experimental values of 1.97 Watts for RUN 34 and 2.59 Watts for RUN 36 compare well with the above predicted values. This indicates that the CL I unstable resonator data is consistent with the stable resonator data.

The time-dependent oscillations in the output beam of the CL I laser employing a confocal unstable resonator all had a period of about 47 ns and increased in amplitude as the fraction of the resonator filled by the saturated gain of a lasing line decreased. A 7 ns oscillation was superimposed on the top of the 47 ns oscillation and is thought to be a mode beat of the laser. The oscillations on lines whose saturated gain does not fill the resonator did not occur for Fresnel numbers less than 3.2. Comparison of CL I and CL II unstable resonator data shows that fewer lines were observed for the CL I which is a consequence of the saturated gain of the CL I being twice as large as that of the CL II. The higher saturated gain of the CL I is also responsible for the large difference in CL I and CL II unstable resonator powers. Overall, the CL I unstable resonator data is consistent with the CL II unstable resonator data.

3.6 CL II OBSERVATIONS OF ALIGNMENT SENSITIVITY

A new alumina discharge tube and new scraper mirrors of much higher quality were used during the CL I unstable resonator experiments. To determine if these new components had any effect on laser performance, it was necessary to first place these components on the CL II and compare new CL II unstable resonator data with old CL II unstable resonator data.

The results indicated no change when using the new components. However, some variations in the initial alignment of the convex mirror led to interesting discoveries about alignment sensitivity. It was found that by adjusting the micrometer controlling the horizontal alignment of the convex mirror, it was possible to increase the power above previously observed values while simultaneously all oscillations disappeared, or it was possible to obtain very strong oscillations (large amplitude) with a lower power. These variations are probably the result of altering the location of the optical

axis; it was no longer parallel to the H_2 injectors. However, the amount of adjustment required to cause these variations was surprising; at most an adjustment of 0.0016 inches on the horizontal micrometer, which translates to an angular variation of 0.040°. Over the mirror separation of 1 meter, this angular displacement alters the beam center on the concave mirror by only 0.70 mm.

IV. CONCLUDING REMARKS

A comparison of the CL I and CL II stable resonator data showed several scale effects. The CL I power was an average of 45% of the CL II power for the same cavity loss, independent of pressure. The fraction of the power in the 1→0 vibrational band did not change significantly; however, the peaks of the power spectral distributions of the CL I were shifted one J lower than the CL II spectral peaks for the same cavity loss. The CL I spectra exhibit fewer J lines than CL II spectra. These effects are a consequence of the fact that the saturated gain of the CL I laser is twice that of the CL II laser when the lasers have the same cavity loss. As observed with the CL II stable resonator data, the CL I spectra shifted toward lower J's as the pressure decreased and shifted toward higher J's as the flow rates increased.

The most interesting result was that, when the saturated gains of the two lasers were the same, the CL I power was an average of 62% of the CL II power for low pressure and 68% for high pressure. For the high SF_6 flow rates, the CL I power was 70-80% of the CL II power, independent of pressure. These data suggest that, if the saturated gain is held constant, for only a 25% performance penalty, the size, weight and gas flow rates of a laser can be reduced by a factor of 2. The power spectral distributions of the two lasers were very similar when the saturated gains of the two lasers were the same. As in the CL II data, the minimum at $P_2(11)$ was observed in the high pressure, high SF_6 flow rate CL I data. This minimum is thought to be a consequence of a near resonant energy transfer[1,2,4] from v = 3, J = 3,4 to v = 2, J = 14 with a subsequent rotational cascade to v = 2, J = 11.

Both the Blaze II and MNORO3SR computer simulations gave good agreement with the measured CL I power, power split and beam diameters. MNORO3SR computations produced power spectral distributions which were in reasonable agreement with the CL I data. These calculations show that the Blaze II and MNORO3SR computer models of the Helios laser are valid as a function of mass flow rates, cavity losses, pressure and size of the laser.

The time-dependent oscillations in the output beam of the CL I laser employing a confocal unstable resonator all had a period of about 47 ns and increased in amplitude as the fraction of the resonator filled by the saturated gain of a lasing line decreased. A 7 ns oscillation, which was superimposed on top of the 47 ns oscillation, is thought to be a mode beat of the laser. The oscillations on lines whose saturated gain does not fill the resonator did not occur for Fresnel numbers less than 3.2. Comparison of CL I and CL II unstable resonator data shows that fewer lines were observed for the CL I which is a consequence of the fact that the saturated gain of the CL I was twice as large as that of the CL II. The higher saturated gain of the CL I also is responsible for the large difference in CL I and CL II unstable resonator powers. Overall, the CL I unstable resonator data is consistent with the CL II unstable resonator data.

The most interesting result of this study was the indication that if the saturated gain is held constant, for only a 25% performance penalty, the size, weight and gas requirements of a laser can be reduced by a factor 2. This was suggested by a comparison of Helios CL I and CL II laser performance with $\alpha_{sat} = 0.0192\ cm^{-1}$. Further experiments need to be performed with other values of α_{sat} to determine if the performance penalty is a function of the magnitude of α_{sat}.

REFERENCES

1. L. H. Sentman, P. Renzoni and S. Townsend, "The Effects of Cavity Losses on the Performance of a Subsonic cw HF Chemical Laser," AAE TR 83-7, UILU Eng 83-0507, Aeronautical and Astronautical Engineering Department, University of Illinois, Urbana, IL, June 1983.

2. L. H. Sentman, M. H. Nayfeh, P. Renzoni, K. King, S. Townsend and G. Tsioulos, "Saturation Effects in a cw HF Chemical Laser," AIAA Journal, Vol. 23, No. 9, 1985, pp. 1392-1401.

3. L. H. Sentman, M. H. Nayfeh, S. W. Townsend, K. King, G. Tsioulos and J. Bichanich, "Time-Dependent Oscillations in a cw Chemical Laser Unstable Resonator," Applied Optics, Vol. 24, No. 21, November 1, 1985, pp. 3598-3609.

4. L. H. Sentman, G. Tsioulos, J. Bichanich and D. Carroll, "An Experimental Study of Fabry-Perot and Stable Resonator cw HF Chemical Laser Performance," AAE TR 85-3, UILU Eng 85-0503, Aeronautical and Astronautical Engineering Departmen , University of Illinois, Urbana, IL, March 1985.

5. L. H. Sentman, W. O. Mosebach and P. Renzoni, "A Theoretical and Experimental Study of cw HF Chemical Laser Performance," AAE TR 81-8, UILU Eng 81-0508, Aeronautical and Astronautical Engineering Department, University of Illinois, Urbana, IL, December 1981.

6. L. H. Sentman and P. Schmidt, "MNORO3: An Efficient Rotational Nonequilibrium cw HF Chemical Laser Model," AAE TR 83-1, UILU Eng 83-0501, Aeronautical and Astronautical Engineering Department, University of Illinois, Urbana, IL, January 1983.

7. L. H. Sentman, P. F. Schmidt and G. M. Marinos, "Effects of the HF Rate Package and the Optical Resonator on cw HF Chemical Laser Performance," AAE TR 83-6, UILU Eng 83-0506, Aeronautical and Astronautical Engineering Department, University of Illinois, Urbana, IL, June 1983.

8. L. H. Sentman, J. D. Bichanich, D. Carroll, V. Coverstone and P. Theodoropoulos, "Simulation of Fabry-Perot and Stable Resonator cw HF Chemical Laser Performance," AAE TR 85-6, UILU 85-0506, Aeronautical and Astronautical Engineering Department, University of Illinois, Urbana, IL, September 1985.

9. J. W. Raymonda, M. Subbiah, J. T. Schimke, S. W. Zelazny and L. H. Sentman, "Advanced HF and DF Chemical Laser Performance Modeling, Vol. I, The CNCDE/BLAZE Rotational Equilibrium Code," TR DRCPM-HEL-CR-79-7, Bell Aerospace Textron, Buffalo, NY, 1979.

10. A. N. Chester and R. A. Chodzko, "Optical Aspects of Chemical Lasers," Ch. 3 of Handbook of Chemical Lasers, ed. by R. W. F. Gross and J. F. Bott, John Wiley and Sons, New York, 1976.